Investigation of Polar Mesosphere Summer Echoes in Northern Scandinavia

Victoria Barabash

IRF Scientific Report 283
February 2004

ISSN 0284-1703
ISBN 91-7305-563-8

INSTITUTET FÖR RYMDFYSIK
Swedish Institute of Space Physics

Kiruna, Sweden

Investigation of Polar Mesosphere Summer Echoes in Northern Scandinavia

Victoria Barabash

Swedish Institute of Space Physics

Kiruna

IRF Scientific Report 283

February 2004

Printed in Sweden

Swedish Institute of Space Physics

Kiruna 2004

ISSN 0284-1703

ISBN 91-7305-563-8

Abstract

This PhD thesis deals with phenomena which are closely related to the unique thermal structure of the polar summer mesosphere, namely Polar Mesosphere Summer Echoes (PMSE). PMSE are strong radar echoes commonly observed by VHF MST radars from thin layers in the 80-90 km altitude interval at high latitudes during summer. They follow a seasonal pattern of abrupt appearance in late May and a gradual disappearance in mid-August. This period corresponds roughly to the time between the completion of the summer time cooling of the polar mesopause to the time of reversal of the mesospheric circulation to autumn condition. In this connection, PMSE are associated with the extremely low temperatures, i.e. below 140 K, which are unique to the polar summer mesopause. Traditional theories of radar (partial) reflection and scattering have been unable to explain the PMSE and the exact mechanism for their occurrence remains unclear despite the steadily increasing interest in them over the past 20 years. Currently accepted theories regarding the mechanism giving rise to PMSE agree that one of the conditions needed for enhanced radar echoes is the presence of low-mobility charge carries such as large cluster ions and ice aerosols which capture the ambient electrons. It has been established that the PMSE are in some way associated with noctilucent clouds (NLC), layers of ice crystals, which constitute the highest observed clouds in the earth's atmosphere. PMSE occurrence and dynamics are also found to be closely connected with the planetary and gravity waves.

Observations of PMSE presented in this thesis have been carried out by the Esrange MST radar (ESRAD) located at Esrange (67°56'N, 21°04'E) just outside Kiruna in northernmost Sweden. The radar operates at 52 MHz with 72 kW peak power and a maximum duty cycle of 5%. The antenna consists of 12x12 array of 5-element Yagis with a 0.7 spacing. During the PMSE measurements the radar used a 16-bit complementary code having a baud length of 1 S. This corresponds to height resolution of 150 m. The sampling frequency was set at 1450 Hz. The covered height range was 80-90 km. The presence of PMSE was determined on the basis of the radar SNR (signal-to-noise ratio). The PMSE measurements have been made during May-August each year since 1997.

PMSE seasonal and diurnal occurrence rates as well as dynamics have been studied in connection with tidal winds, planetary waves, temperature and water vapor content in the mesosphere (Papers I, IV and VI). Simultaneous and common-volume observations of PMSE and noctilucent clouds have been performed by radar, lidar and CCD camera (Paper V). Correlation between variations in PMSE and variations in extra ionization added by precipitating energetic electrons or high-energy particles from the Sun has been examined (Papers II and III). Possible influence of transport effects due to the electric field on PMSE appearance has been studied during a solar proton event (Paper III).

Keywords: Polar Mesosphere Summer Echoes, middle atmospheric dynamics, ionospheric disturbances, solar radiation, aerosol, MST radar, planetary waves, noctilucent clouds.

Contents

1. Introduction **5**

2. Thermal and dynamical structure of the upper mesosphere and lower thermosphere in high latitudes **6**
2.1 Vertical structure of the neutral atmosphere 6
2.2 Mean temperatures in the upper mesosphere and lower thermosphere 6
2.3 Dynamical structure of the upper mesosphere and lower thermosphere 9

3. Polar Mesosphere Summer Echoes **11**
3.1 Definition of Polar Mesosphere Summer Echoes 11
3.2 Seasonal occurrence 12
3.3 Diurnal variation 12
3.4 Observational frequencies 14
3.5 Latitudinal observations 14

4. Connections with other phenomena **15**
4.1 Noctilucent clouds 15
4.2 Waves 16
4.3 Charged aerosols 18

5. MST radar observation of the upper atmosphere **20**
5.1 Scattering and reflection of MST radar signals in the upper atmosphere 20
5.2 Esrange VHF MST radar (ESRAD) 24

6. Summary of the included papers **26**

Bibliography **29**

Acknowledgements **35**

Acronyms **36**

Included papers

1. Barabash, V., Chilson, P., Kirkwood, S., Rechou, A., and Stebel, K., Investigations of the possible relationship between PMSE and tides using a VHF MST radar, Geophysical Research Letters, 25, 17, 3297-3300, 1998.

2. Barabash, V., Kirkwood, S., and Chilson, P., Are variations in PMSE intensity affected by energetic particle precipitation?, Annales Geophysicae, 20, 539-545, 2002

3. Barabash, V., Kirkwood, S., Feofilov, A., and Kutepov, A., Polar Mesosphere Summer Echoes during the July 2000 Solar Proton Event, Annales Geophysicae (in press), 2003.

4. Kirkwood, S., Barabash, V., Chilson, P., Rechou, A., Stebel, K., Espy, P., Witt, G., and Stegman, J., The 1997 PMSE season - its relation to wind, temperature and water vapor, Geophysical Research Letters, 25, 11,1867-1870, 1998.

5. Stebel, K., Barabash, V., Kirkwood, S., Siebert, J., and Fricke, K.H., Polar mesosphere summer echoes and noctilucent clouds: Simultaneous and common-volume observations by radar, lidar and CCD camera, Geophysical Research Letters, 27, 5, 661-664, 2000.

6. Kirkwood, S., Barabash, V., Brändström, U., Moström, A., Stebel, K., Mitchell, N., and Hocking, W., Noctilucent clouds, PMSE and 5-day planetary waves: a case study, Geophysical Research Letters, 29, 10, 10.1029/2001Gl014022, 1-4, 2002.

Non included papers

1. Rechou, A., Barabash, V., Chilson, P., Kirkwood, S., Savitskaja, T., and Stebel, K. Mountain wave motions determined by the Esrange MST radar, Annales Geophysicae, 17, 957-970, 1999.

2. Kirkwood, S., Barabash, V., Belova, E., Nilsson, H., Rao, T. N., Stebel, K, Osepian, A., and Chilson P., Polar mesosphere winter echoes during solar proton event, Adv. In Polar Upper Atm. Res., Japan, 2002.

1. Introduction

This thesis deals with a phenomenon, which is closely related to the thermal structure of the polar summer mesopause and called Polar Mesosphere Summer Echoes (PMSE). PMSE are strong radar echoes, which appear between 80-90 km altitudes in high latitudes (Ecklund and Balsley, 1981; Röttger et al., 1988) and mid-latitudes (Czechowsky et al., 1979; Reid et al., 1989; Thomas et al., 1992; Chilson et al., 1997) during the summer months. At high latitudes, i.e. above 60°N, they were first reported by Ecklund and Balsley (1981) as abnormally strong and persistent radar returns from the mesopause region (around 85 km altitude) above Alaska during the mid-summer months. Since that time there has been a growing interest in this phenomenon.

The mesopause region is characterized by extremely low temperatures falling to below 140 K in the polar summer, whereas during the winter months the mesopause temperatures are around 190 K. Considering that the polar atmosphere is continuously illuminated in the summer months, and is in total darkness for several months in the winter, it might be expected the reverse relationship. However, this unique thermal feature has been interpreted as being the result of a mean global circulation with upwelling air masses above the summer pole, sinking masses above the winter pole, and a mean meridional circulation from the summer to the winter pole. This mean circulation thought to be driven by the deposition of momentum of breaking gravity waves and therefore, represents a complicated balance between energy and momentum sources and sinks (Garcia and Solomon, 1985; Berger and Von Zahn, 1999; Akmaev, 2001; Zhu et al., 2001). An analysis of the thermal and dynamical structure of the mesopause region, i.e. at altitudes between 80 and 90 km, in high latitudes is given in Section 2.

An overview of PMSE seasonal and diurnal occurrence rates, frequency and latitudinal observations is presented in Section 3.

PMSE connection to other phenomena such as planetary and gravity waves, noctilucent clouds (NLC) is discussed in Section 4. Many observations of PMSE have been made using radar, lidar, and rockets, but the nature of the scattering processes and their generating mechanism remain an open question. For the present time the explanations given for PMSE are mostly related to small-scale fluctuations in electron number density, which creates refractive index variations at the Bragg scale (= radar half wavelength, 3 m for a 50 MHz radar). These fluctuations thought to be maintained by charged aerosols. Recent developments on the possible role of charged aerosols in PMSE appearance are outlined in Section 4.

PMSE have mostly been observed with MST (mesosphere-stratosphere-troposphere) radars, which were introduced in the 1970s for observations of the structure and dynamics of the lower and middle atmosphere. These radars operate usually near 50 MHz and detect echoes from turbulence-induced irregularities and gradients of the refractive index (Woodman and Guillen, 1974). Description of the MST radar techniques and analysis of scattering and reflection processes are discussed in Section 5.

The papers included in this thesis represent studies gathering direct measurements of PMSE in the northern Scandinavia and important background parameters such as winds (Papers I, IV), waves (Paper VI), temperature (Papers IV, VI), additional ionization (Papers II and III) and electric fields (Paper III). PMSE connection with noctilucent clouds is described in Papers V and VI. The measurements of PMSE have been made using the Esrange VHF MST Radar (ESRAD) at 67°53'N, 21°06'E. They were complemented by the ground-based observations (from lidars, riometers, magnetometers, CCD cameras, meteor radar SKiYMET, interferometer), observations from space (energetic particles spectra from NOAA GOES-10 and ACE satellites, water vapor from HALOE instrument on board of UARS satellite, CO_2 volume mixing ratio from CRISTA1 and 2 satellites), amateur observations (noctilucent clouds) and assimilations (from UK Meteorological Office (UKMO) models, MSISE-90 and energy deposition and ion-chemical models).

2. Thermal and dynamical structure of the upper mesosphere and lower thermosphere in high latitudes

2.1 Vertical structure of the neutral atmosphere

The neutral atmosphere is usually divided into altitude zones according to the temperature profile: the troposphere which absorbs infrared radiation from the ground and where the temperature decreases with height; the stratosphere where the temperature increases mainly due to ozone absorption of solar UV radiation; the mesosphere where only a small amount of radiation is absorbed and the temperature decreases again; the thermosphere where the temperature increases because of the absorption of solar short-wave radiation (< 4 mm) by all atmospheric components (Figure 2.1). The atmosphere below 100 km is well mixed, with a composition much like that at sea level, i.e. N_2 (80%) and O_2 (20%), except for minor components. This is the homosphere. Above 100 km in the heterosphere a mean free path of constituents becomes larger than turbulent displacements, so the gases can be separated by molecular diffusion more rapidly than they are mixed by turbulence, and the composition varies with altitude.

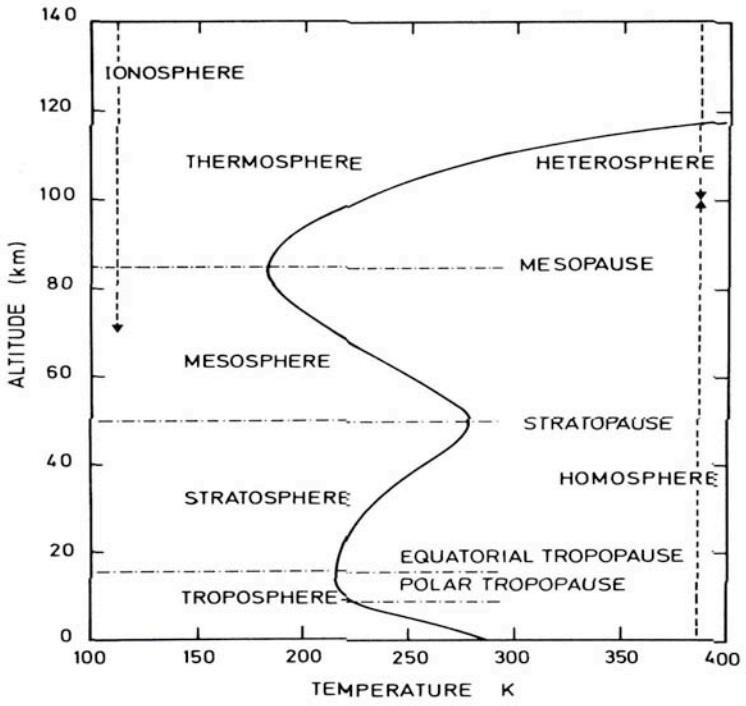

Figure 2.1. *Thermal structure of the neutral atmosphere (Brasseur and Solomon, 1986).*

2.2 Mean temperatures in the upper mesosphere and lower thermosphere

The mesopause is the boundary between the mesosphere and thermosphere corresponding to the temperature minimum. The mean seasonal variations of the mesopause temperature and altitudes at 69°N are shown in Figure 2.2. The remarkable feature of the mesopause is that it is much colder in summer than in winter, particularly in the polar region. The mean summer mesopause (May-August) is located at approximately 85-88 km and reveals a mean temperature as low as 130 K, the winter temperatures (September-April) are considerably higher, i.e. about 190 K, and the mesopause is located around 98 km (Lübken and von Zahn, 1991).

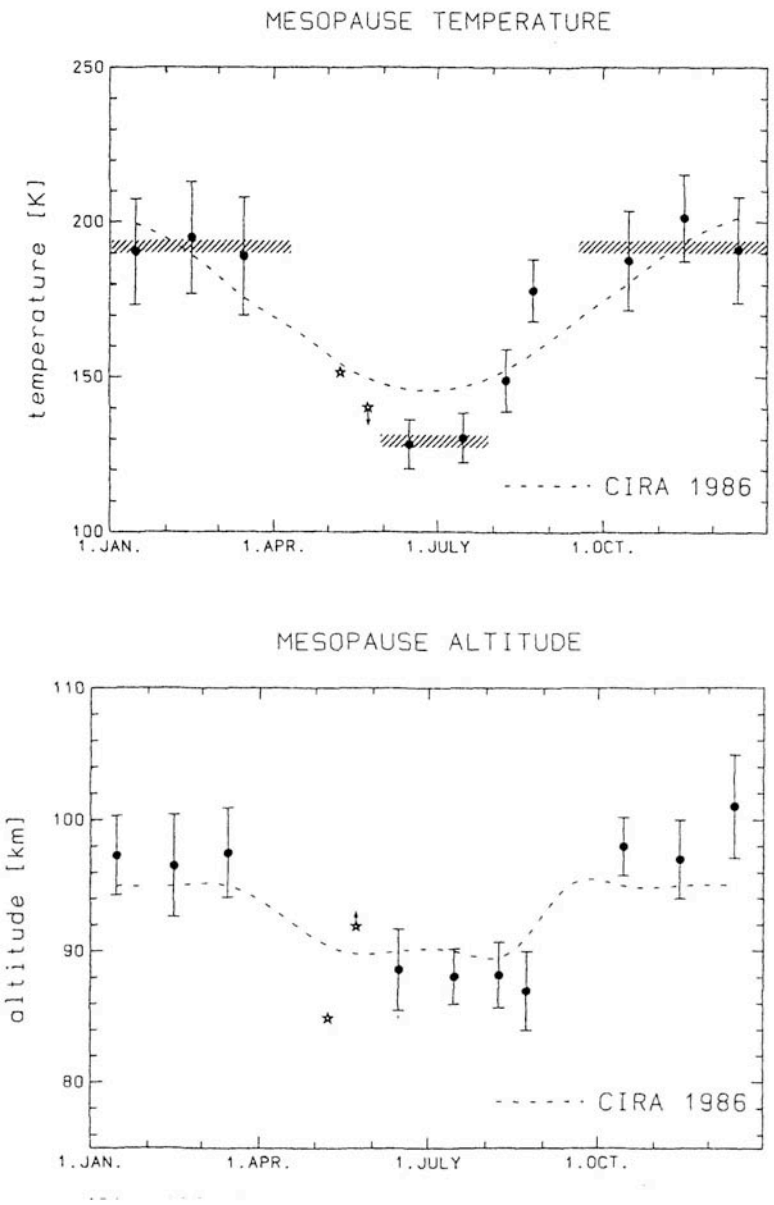

Figure 2.2. *Temperature and altitude of the mesopause at 69°N as functions of season. The vertical bars give the variability of the temperature and altitude in that particular month (Lübken and von Zahn, 1991).*

This behavior is interpreted today as being the result of a large scale circulation with upwelling air masses over the summer pole, which flow towards the winter pole some where above the mesopause and sink again into the lower part of the atmosphere over the winter pole (Andrews et al., 1987). As the air rises it moves into the region of lower pressure with consequent expansion, leading to a temperature drop and subsequently to the cold summer mesopause. This mesopause circulation thought to be forced by atmospheric gravity waves. The gravity waves are excited for example by the tropospheric winds flowing over the mountains, by convection and weather fronts in the troposphere and regions of shear instability. The wind typical speeds are of 0-20 ms^{-1}, and thereby the gravity waves are expected to have similar phase speeds.

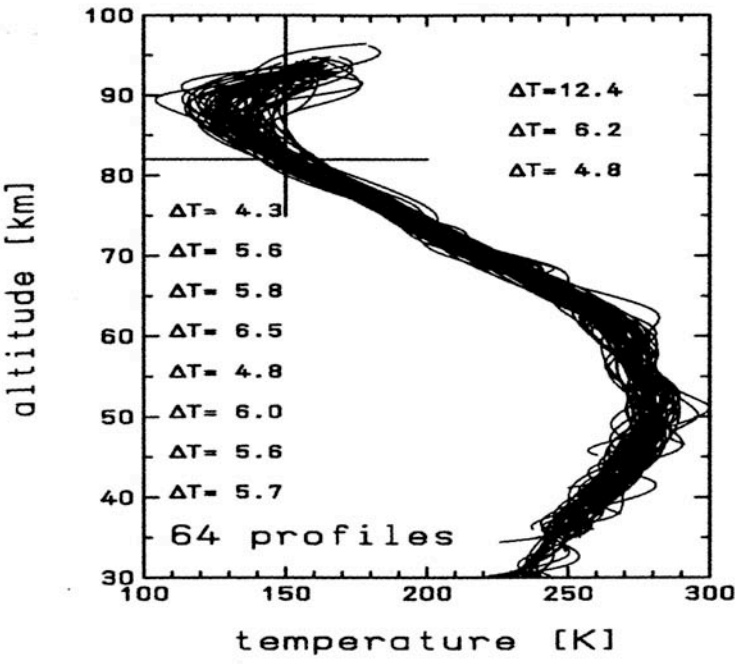

Figure 2.3. *Temperature profiles observed from mid-May until mid-August in 1987, 1991, 1992, 1993, 1995, 1997. The temperature of 150 K at 82 km has been marked by the solid line. The numbers given at various altitudes indicate the standard deviation at that height (Lübken, 1999).*

The lower altitude winds, which change direction between winter and summer, allow only those gravity waves moving against the mean flow to propagate upwards into the atmosphere. Namely, they filter the gravity waves in such way that the waves are predominantly eastward in the summer and westward in the winter. The wave amplitudes grow as exp(z/2H), z is the height and H is the density scale height. This can be understood if we consider that the kinetic energy of the wave is proportional to $\rho_o V_z^2$, where ρ_o is the density at the excitation level of the disturbance and V_z is the velocity in z-direction. While the density decreases with increasing z as exp(-z/H), the amplitude of the wave has to increase like exp(z/2H) to maintain energy conservation. The wave amplitudes grow until the horizontal disturbance speeds match the difference between background wind speed and phase speed. At these so-called saturation levels the waves start to break. When the waves break in the upper atmosphere, their momentum is deposited to the background winds and acts to decelerate the mean flow. Reid et al. (1988) suggested that the most intense wave breaking occurred above 86 km, the place where the temperature variance is more significant than at lower heights (Lübken et al., 1996).

In Figure 2.3 individual temperature profiles observed from mid-May until mid-August in various years (1987, 1991, 1992, 1993, 1995, 1997) demonstrate rather small variability. The variability increases toward the upper part of the profile, which has been explained by both the uncertainties in the measurement technique (Lübken, 1999) and increased temperature variability induced by turbulent activity (Lübken et al., 1997).

The summer mesopause temperature and altitude vary with latitude. Thus, moving from 69°N to 78°N the mesopause temperature decreases by 6-8 K in late July and August, and the mesopause altitude increases by 1 km (Lübken and Müllemann, 2003). This has been partly explained by the later transition from summer to winter at very high latitudes (78°N).

2.3 Dynamical structure of the upper mesosphere and lower thermosphere

The thermal structure of the upper mesosphere and lower thermosphere is closely connected with its dynamics, which is determined by the prevailing winds, tides and waves. Studies of the mean winds and tides of the upper mesosphere and lower thermosphere region at polar latitudes have been undertaken by ground-based radar techniques, i.e. meteor radar, medium-frequency (MF), mesosphere-stratosphere-troposphere (MST) and incoherent scatter radars (Manson and Meek, 1991; Virdi and Williams, 1993; Portnyagin et al., 1993a, 1993b; Kirkwood and Rechou, 1998; Manson et al., 1999; Portnyagin and Solovjova, 2000; Hocking, 2002; Mitchell et al., 2002; Kirkwood et al., 2000 (Paper VI); Manson et al., 2003; Kirkwood and Stebel, 2003).

The prevailing zonal and meridional winds derived from the 32.5 MHz Meteor Wind Radar located at Esrange (68°N, 21°E) are shown in Figure 2.4. The dominating zonal pattern in the upper part of the polar summer mesosphere is the westward wind system and the region of eastward wind system above. In contrast, the winter winds are eastward at all heights. The equinoxes appear as rather extended transitions between the summer and winter flow. The zonal winds show the rather abrupt change of circulation from winter (eastward) to summer (westward), and a slow return to winter circulation. The meridional prevailing wind contains the southward flow at all heights for summer months. The regions of northward flow occur at around the autumnal equinox and in April (Mitchell et al., 2002; Manson et al., 2003). This circulation pattern is connected with vertical movements and compensates the reverse solarly driven meridional circulation in the stratosphere and lower mesosphere below.

The wind pattern in the mesosphere and lower thermosphere is strongly affected by tides, planetary waves and gravity waves. These waves interact with each other and with the mean winds, driving the mean wind flow to states far removed from those predicted by considerations of pure radiative equilibrium.

Tidal motion consists mainly of semidiurnal (12-hour) and the diurnal (24-hour) periods. The semidiurnal (12-hour) and the diurnal (24-hour) tides are waves of zonal wave number 2 and of zonal wave number 1, respectively, which propagate westward following the apparent motion of the Sun. Wave number is defined as a ratio between the Earth's circumference and wavelength. The diurnal tide has a period of 24 hours and covers the Earth's circumference at the observer latitude in 24 hours. Such a tide has wave number 1. The semidiurnal tide has a period of 12 hours but also covers the circumference in 24 hours and has wave number 2. The main source of solar tides is the daily variation of solar radiation absorbed by oxygen in the thermosphere, by ozone in the troposphere and mesosphere. Lunar tides are driven by lunar gravitational forcing and have amplitudes typically only a few percent those of solar tides (Richmond, 1995). Observations of the 12- and 24-hour tides in the polar mesosphere/thermosphere region (68°N, 21°E) reveal a clear seasonal cycle in amplitude and phase. The phase values are the time of the first maximum of wind for the appropriate component, measured in local time. For the semidiurnal tide the amplitude of the zonal and meridional components are similar over the year and gain its maximum in August-September and in January (Mitchell et al., 2002). The semidiurnal tidal phase is relatively constant during the summer (April-August), decreases to earlier hours in October, then advances to later hours in November-December, and finally declines to the April values. The diurnal tide exhibits more complicated behavior with asymmetries between the zonal and meridional components in both amplitude and phase. In particular, the meridional amplitudes are generally larger than the zonal amplitudes particularly at the upper heights in July-August. The zonal and meridional phases have sharp transitions with height over the course of the year (Mitchell et al., 2002; Manson et al., 2003).

(a)

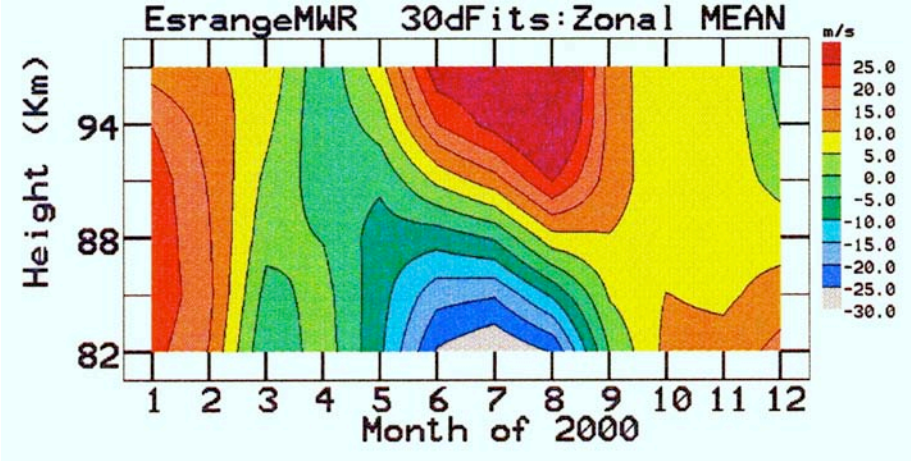

(b)

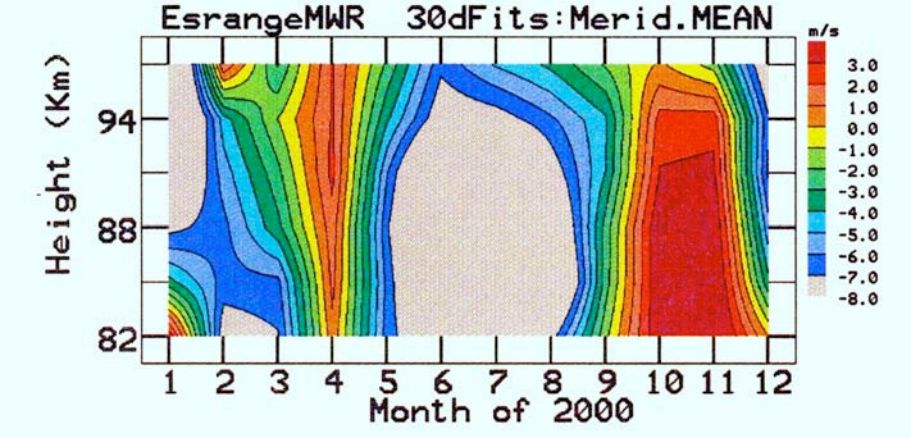

Figure 2.4. *Monthly mean zonal (a) and meridional (b) winds measured by the 32.5 MHz Meteor Wind Radar at Esrange. Positive values represent eastward (a) and northward (b) winds. Negative values represent westward (a) and southward (b) winds (Manson et al., 2003).*

Wind oscillations with periods 2, 5, 10 and 16 days are referred to planetary wave activity and exhibit strong interannual variability (Jacobi et al., 1998; Kirkwood et al., 2002 (Paper VI); Manson et al., 2003; Kirkwood and Stebel, 2003). The waves are more intensive during the winter months (Jacobi et al., 1998; Williams and Avery, 1992; Manson et al., 2003). Their amplitudes might exceed 5 ms^{-1} for 16-d and 10 ms^{-1} for 5-d and 2-d waves as well as be extended through 70-95 km height interval. However, the wave propagation might be minimized by strong winds (Luo et al., 2000; 2002) and there might be non-linear interactions between tides and planetary waves in the mesopause region. (Rüster, 1994).

Atmospheric disturbances supported by the positive restoring force of buoyancy are known as gravity waves. According to different studies gravity wave periods in upper mesosphere in northern Scandinavia vary from 30 min-2 hours up to 6-8 hours (Manson et al., 2003; Rapp et al., 2003a). The gravity waves are able to transport momentum and energy between different atmospheric layers, and thus, affect the thermal structure of the upper atmosphere (Medvedev and Klaassen, 2003) and the mean distribution of chemical species (Jiyao Xu et al., 2003).

It should be mentioned that, the spatial and temporal variability of the wind and wave field of the mesosphere and lower thermosphere in high latitudes still remains one of the not well-understood aspect of atmospheric dynamics.

3. Polar Mesosphere Summer Echoes

3.1 Definition of Polar Mesosphere Summer Echoes

Polar Mesosphere Summer Echoes (PMSE) are strong radar echoes commonly observed by VHF (Very High Frequency) radars at high latitudes, i.e. above 60°N, from heights between 80-90 km. This phenomenon was discovered in 1979 by Ecklund and Balsley (1981) who reported strongly enhanced radar backscatter detected during the polar summer by 50 MHz radar at Poker Flat, Alaska. At mid-latitudes mesosphere summer echoes were first observed by the 53.5 MHz SOUSY radar (52°N) in northern Germany (Czechowsky et al., 1979). The PMSE layers often occur in double or multiple structures separated by several kilometers and can be as thin as the radar resolution of 150 m up to several kilometers (Franke et al., 1992). The average signal peak is located at 86 km (Ecklund and Balsley, 1981). Layers are frequently observed to oscillate up and down in altitude by up to a few kilometers, yielding vertical velocities of 8-10 ms^{-1} over timescales of 6-20 minutes (Röttger et al., 1990d). On longer timescales (hours) the layers mostly move downward by 1-2 kmh^{-1}.

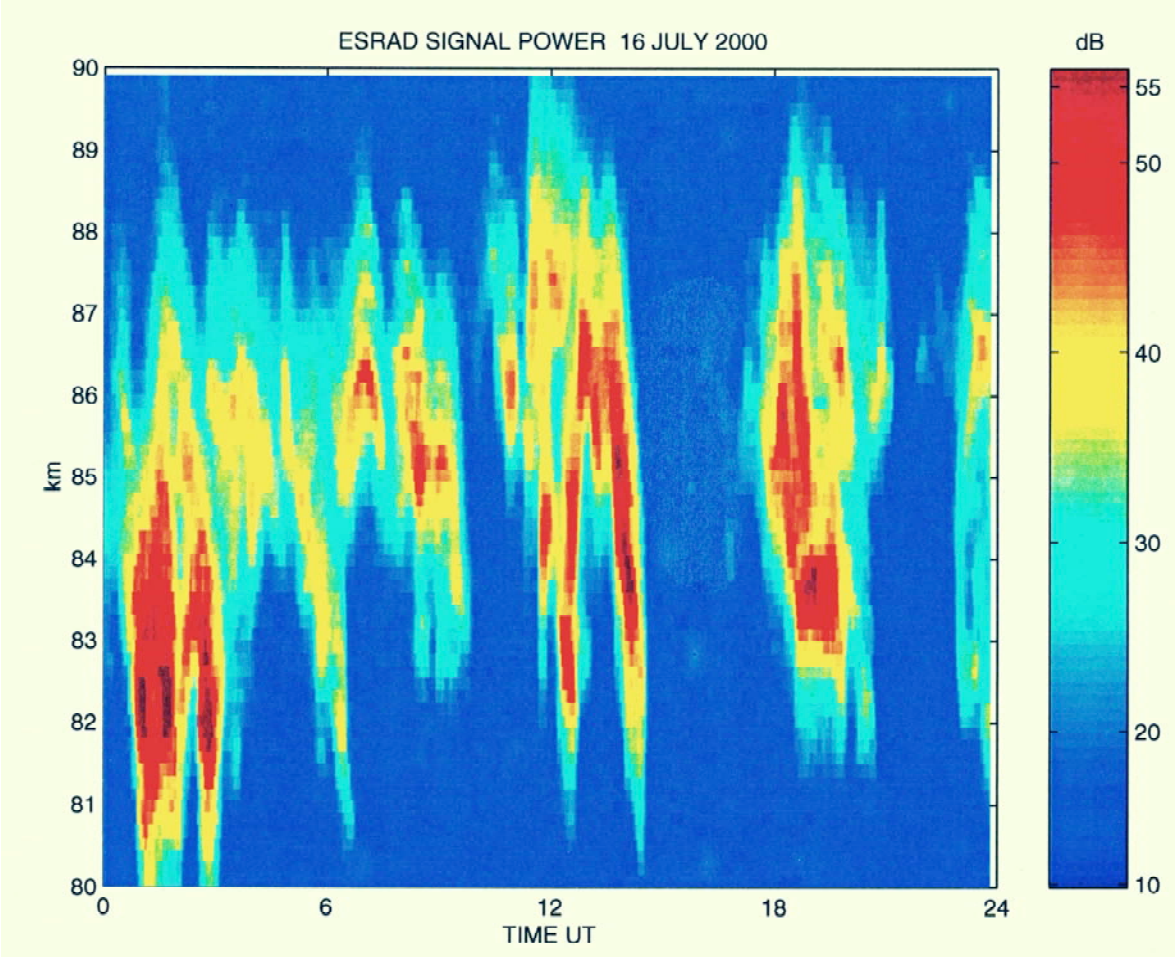

Figure 3.1. *PMSE observed by Esrange VHF MST radar (ESRAD). Signal power versus altitude and time for 16 July 2000.*

3.2 Seasonal occurrence

The seasonal variation of PMSE in the northern hemisphere shows a steep increase in occurrence at the end of May and slow fade-out in mid-August (Balsley et al., 1983; Kirkwood et al., 1998 (Paper IV); Barabash et al., 1998 (Paper I)) or in late July (Hoffmann et al., 1999). This behavior is strongly connected to extremely low temperatures, i.e. below 130 K, in the mesopause region supported by seasonal wind circulation, when the zonal wind changes direction from eastward (winter) to westward (summer) (Kirkwood et al., 1998 (Paper IV)). This aspect has been briefly discussed in Section 2. Here, we would like to emphasis that, the change in stratospheric circulation means a change in wave filtering, by the background winds, i.e. the gravity waves with the eastward phase velocity would propagate up during the summer and the waves with the westward phase velocity would propagate up during the winter.

Another factor that might control the seasonal occurrence of PMSE is a water vapor. Water vapor availability show an increase during the summer, possibly taking place in late May, at the time of PMSE start (von Zahn, 1997; Kirkwood et al., 1998 (Paper IV)) and remains high up to first part of the declining PMSE season. Typical mean mixing ratios in July vary from 4.1 ppmv (parts per million by volume) to 0.5 ppmv at 75 km and 93 km, respectively. In the upper mesosphere water vapor content increases slightly by 1 ppmv from July to August (Körner and Sonnemann, 2001). Combination of temperature and water vapor content determines conditions for formation of ice aerosols, which are thought to be a very important factor in creating PMSE. Namely, if the degree of saturation S that is the ratio between the partial pressure of water vapor P_{H2O} and the saturation pressure of water vapor over ice P_{sat} is more than 1, the particles can exist or grow. If S is less than 1, the particles will evaporate. The saturation pressure of water vapor over ice P_{sat} in (N/m^2) is determined according to Marti and Manersberger (1993):

$$\log_{10} P_{sat} = 12.537 - \frac{2663.5}{T}$$

From this equation it is seen that, when less water vapor is available as that is in early May, lower temperatures would be needed to allow ice aerosols to form, otherwise the aerosol might not form before the temperature is forced above some threshold value. Ice particles can exist or grow in an altitude range from approximately 82 to 92 km in midsummer. Lübken and Müllemann (2003) derived supersaturation values of $S > 40$ or even $S > 100$ which might occur around the summer mesosphere. Nevertheless, the altitude range for $S > 1$ shrinks with progressing season and disappears at the end of August. This led to the idea that aerosol availability might determine the PMSE seasonal appearance.

3.3 Diurnal variation

The diurnal variation of PMSE has a marked semidiurnal character with a prominent minimum around 19:00-22:00 UT and maximum around 12:00-13:00 UT (Balsley et al., 1983; Czechowsky et al., 1989; Barabash et al., 1998 (Paper I); Hoffmann et al., 1999; Barabash et al., 2002 (Paper II)) (Figure 3.2). These maxima and minima are stable through the whole season. Secondary maxima might occur in the early morning hours, but are not so stable in time (Hoffmann et al., 1999).

The explanations of the PMSE semidiurnal variation include tidal temperature changes (Hoffmann et al., 1999) and temperature induced ice-aerosol modulations (Kirkwood and Rechou, 1998; Rüster, 1995). The tidal temperature changes thought to be induced by meridional

tidal winds transporting cold (warm) air from polar (equatorial) latitudes to the observational place. Hoffman et al. (1999) found a correlation with a time shift of 3 hours between SNR (signal-to-noise ratio) and meridional wind component from radar observations at Andenes, at 85.7 km 10 June-7 July 1996. However, the zonal and meridional winds vary with height, which might be connected with interactions between different tidal modes (Barabash et al., 1998 (Paper I)). So, more studies on, for example, common volume and simultaneous temperature measurements supported by modeling of tides would be necessary to resolve this question.

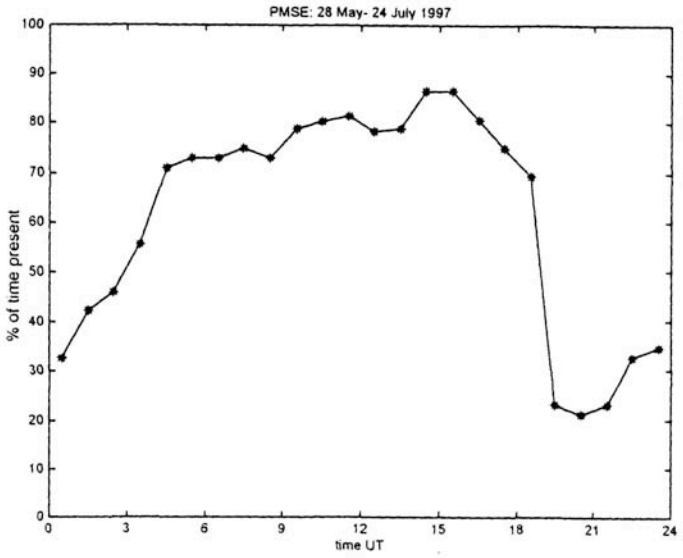

Figure 3.2. *Occurrence rate of PMSE during the period 28 May-24 July 1997 as a function of time of day (Barabash et al., 2002 (Paper II)).*

Another possibility remains that tidal or some other effects on aerosols may be involved in the variability of PMSE, since the presence of ice aerosols and large cluster ions has been found to be a necessary (but not sufficient) factor for PMSE production (Cho and Röttger, 1997). Studies of PMSE during the solar proton event demonstrated such possibility (Barabash et al., 2003 (Paper III)). Namely, it has been shown that, the northward component of the electric field in the upper atmosphere might produce upward/downward transport of ions and aerosols, thus possibly decreasing the amount of charged aerosols in the vicinity of PMSE. The intensification of the northward component of the electric field at the time of greatest geomagnetic disturbances coincided with a substantial decrease of the PMSE strength above 86 km. So, it was proposed that it is transport effects due to the intensified electric field can be responsible for the PMSE modification.

The situation becomes more complicated when the PMSE variability could be modified by extra ionization, added by precipitating energetic electrons from the magnetosphere or high-energy particles from the Sun. A number of investigations has been made on the possible relationship between PMSE and absorption of radio noise from the stars ("cosmic noise") in the ionosphere registered by a riometer (Klostermeyer, 1999; Bremer et al., 2000; Barabash et al., 2002 (Paper II); Barabash et al., 2003 (Paper III)). Particularly Barabash et al. (2002) (Paper II) found that the mean diurnal variation of the square of absorption and the linear PMSE are intensity highly correlated, but their day-to day variations showed significant correlation only during the late evening hours, i.e. around a semidiurnal minimum. This meant that no more than 20% of the day-to-day PMSE variation could be statistically explained by the variation in cosmic

noise absorption. And thus, the ionization cannot be considered as a primary source of varying PMSE.

3.4 Observational frequencies

PMSE have been observed in the frequency range from 2.78 MHz (Bremer et al., 1996) and 8-9 MHz (Karashtin et al., 1996) to 224 MHz (Hoppe et al., 1988; Röttger et al., 1988; Röttger and La Hoz, 1990b) and 933 MHz (Röttger et al., 1990c). That is why the refractive index irregularities responsible for radar echoes have to exist at scales of half the radar wavelength, i.e. between 50 m and 16 cm. It is very unlikely that the same properties of irregularities can cause the scattering over these wide ranges and PMSE are likely to comprise a complex of different mesospheric phenomena. Röttger (1995) suggested five classes of possible phenomena, which might be responsible for mesospheric echoes: steep gradients of electron density (several MHz), neutral turbulence (a few 10s of MHz), enhanced electron density fluctuations and electrostatic waves (10 - 100 MHz), dressed heavy ions and aerosols (1 GHz). Comparison of scatter cross sections at different frequencies might serve as an essential tool to investigate dynamics and aeronomy of the upper atmosphere, and thus to extend our knowledge of PMSE origin.

3.5 Latitudinal observations

PMSE are usually observed at latitudes above 60°N. However, they have been observed as far south as 52°N in the Harz mountains in Germany with 53.5 MHz SOUSY radar (Czechowsky et al., 1979), and 52.4°N in Aberystwyth, Wales by 46.5 MHz radar (Thomas and Astin, 1994). As a historical note, we mention that the observations made by Czechowsky et al. (1979) predate those of Ecklund and Balsley (1981). That is, enhanced radar echoes associated with the summer mesopause region were actually first detected at mid-latitudes. Although similar to PMSE, the frequency of occurrence of mid-latitude mesospheric summer echoes is considerably smaller, they tend to be shorter in duration and be restricted to day-time (Latteck et al., 1999), and their backscatter enhancement is not as pronounced. This is most likely due to the fact that the ambient temperature of the summer mesopause increases with decreasing latitude, thus reducing the chances of ice particle forming (Chilson et al., 1997). However, the necessary low temperature could be created by gravity waves, as it has been proposed by Chilson et al. (1997) with mid-latitude radar and lidar observations in the Harz mountains. Another possibility remains for echoes appearance at higher temperatures is the presence of large aerosols or hydrated ions (Kelley et al., 1987).

In the southern hemisphere PMSE have been observed at 62°S over King George Island, Antarctica with 50 MHz radar (Woodman et al., 1999). Observations of PMSE at high latitudes in northern and southern hemispheres show a significant difference in occurrence rate and intensity (Woodman et al., 1999). The southern-hemispheric PMSE are more sporadic and 34-44 dB weaker than PMSE in northern hemisphere (Balsley et al., 1995; Woodman et al., 1999). Possible explanations of these peculiarities have been attributed to higher mesopause temperatures (Thomas, 1995; Huaman and Balsley, 1999) and weaker mesospheric winds (Vincent, 1994; Huaman and Balsley, 1999) in the southern hemisphere. Vincent (1994) suggested that PMSE's reduced occurrence may also be related to reduced gravity wave activity and the resulting reduced mesospheric circulation.

4. Connections with other phenomena

4.1 Noctilucent clouds

PMSE layers have been quite often (but not always) found to be coupled to noctilucent clouds (NLC). The name of the clouds means the clouds which shine in the night. They are seen as they are lit up from below by the Sun from latitudes between about 55°N and 65°N. In the polar summer night, the sunlight is reflected from NLC at low angles, making them visible from much further south than where are located. At the same time since the Sun never gets sufficiently far enough below the horizon, NLC are nor directly visible from the ground from latitudes higher than about 65°N.

Figure 4.1. *NLC in Moscow region, 25-26 June 1996 (Photo by P. Dalin).*

These clouds occur during summer at high and mid-latitudes around 81.5-85.5 km (Witt, 1962). Comparison of seasonal occurrence rate of PMSE and NLC demonstrated a delay of NLC appearance until the period of lowest temperatures was well established in later summer months, and PMSE were also present throughout the day (Kirkwood et al., 1998 (Paper IV); Fiedler et al., 2002). The temperature measurements performed by the meteorological rockets reveal that the temperature in the NLC layer might be lower than 154 K (Lübken et al., 1996). The strong similarities in occurrence properties between the NLC and the PMSE layers support the hypothesis of their common origin. The NLC clouds most likely consist of large ice aerosols (40-1000 nm) and may require several hours or days to form (Gadsden and Schröder, 1989)**.** Whereas PMSE are thought to be due to much smaller charged aerosols or water cluster ions which should form more quickly. The appearance of PMSE and NLC at the overlapping altitude and same season makes it very likely that both phenomena might have a common origin and be controlled

by common processes. To clarify this question an attempt to classify the PMSE and NLC coupling has been made by the simultaneous and common-volume observations of these two mesospheric phenomena. Nussbaumer et al. (1996) distinguished between the tight and loose coupling of the two. In the first case the NLC fitted the lower boundary of PMSE (Fig. 4.2). In the second case the NLC exhibits gaps in appearance lasting more than 1 hour. Von Zahn and Bremer (1999) classified three types of joint NLC / PMSE events depending on their temporal and spatial differences. Type 1 (standard case) includes: (1a) while NLC is present, PMSE occur simultaneously in the same volume, (1b) the NLC layer is considerably narrower than the PMSE layer, (1c) the lower ledges of the NLC and PMSE layers coincide. Type 2 (with temporal differences between the layers) is like type 1, but at times NLC are present without PMSE. Type 3 (with spatial differences between the layers) is like type 1, but at times the NLC is not at the lower edge of PMSE.

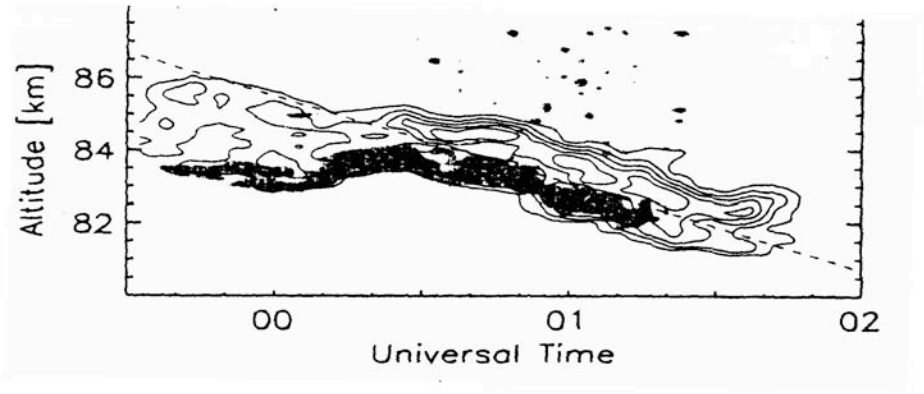

Figure 4.2. *Contours of signal strength for NLC/PMSE event of July 30-31 1994, obtained from the ALOMAR SOUSY radar and Bonn University lidar. Radar data are shown as solid lines with SNR = 5, 10, 15, 20, 25 dB. Lidar data are shown as black areas backscatter ratio above 20 (Nussbaumer et al., 1996).*

Stebel et al. (2000) (Paper V) have also observed the loosely coupled layer types similar to that described by Nussbaumer et al. (1996). Simultaneous observations made by lidar and a CCD camera revealed a transition between two NLC bands with a different spatial orientation. The orientation of the NLC bands has been found to be consistent with changes in the wind direction derived from the 50 MHz Esrange MST radar (ESRAD) observations that has been interpreted as an advection of different air masses during the same event.

4.2 Waves

PMSE observations show a variety of dynamic features. Long-period (5-10 hours) waves and tidal components were first noted to be related to the occurrence and echo power of PMSE by Carter and Balsley (1982) and Balsley et al. (1983). Later studies quantified these relations, but were quite different in their interpretation. Rüster (1995) and Cho and Morley (1995) invoked wave-induced temperature changes as a possible link between the PMSE and wave dynamics. Williams et al. (1995) attribute to wave induced shear instabilities. In support of the latter explanation, Fritts et al. (1988) suggested that the maximum of echo power occurs preferentially in regions of small gradient Richardson number, i.e. the gradient Richardson number is close to or slightly smaller than 0.25, induced by dynamical instabilities associated with the background wave field. The gradient Richardson number R_i reflects the dynamical stability of the mean flow,

so it provides a criterion for the onset of turbulence (Salby, 1996). It can be calculated through the expression:

$$R_i = \left[\frac{g}{\theta} \Big/ \left(\frac{\partial u}{\partial z} \right)^2 + \left(\frac{\partial v}{\partial z} \right)^2 \right],$$

where g is the gravitational acceleration of 9.806 ms^{-2}, θ is the potential temperature, z is the altitude, u and v are the zonal and meridional components of the wind, respectively. Potential temperature θ is the temperature assumed by the system when compressed or expanded adiabatically to a reference pressure $p_o=10^3$ mb:

$$\theta = T \cdot \left(\frac{p_o}{p} \right)^k, \quad k = \frac{R}{C_p},$$

where T is the absolute temperature in K, p is the atmospheric pressure in mb, R is the universal gas constant 8.314 $Jmol^{-1}K^{-1}$, Cp is the isobaric specific heat capacity $1.005 \cdot 10^3$ $Jkg^{-1}K^{-1}$ for dry air at 273 K (Salby, 1996).

Czechowksy et al. (1989) and Barabash et al (1998) (Paper I) noted, that PMSE power did not always correlate with wind shear. Particularly, a study of PMSE using the SOUSY VHF radar (Czechowksy et al., 1989) demonstrated that only the weaker echoing regions of PMSE are related to the background wind shear. On the other hand, Barabash et al. (1998) (Paper I) has found that strong wind shears which tend to increase through the season and reach values of 200 $ms^{-1}km^{-1}$ for some height above 85 km shows a lack of correlation with PMSE echo power registered by Esrange MST radar (ESRAD). This discrepancy might be partially explained by differences in power aperture products of ESRAD and the SOUSY radar making detection of low scattered power by ESRAD difficult.

Another aspect concerning the possible relation between the PMSE and waves is the motion of PMSE layers which has been related to the presence of short-period gravity waves (Röttger, 1994; Pan and Röttger, 1996; Chilson et al., 2000). Figure 4.3 represents such a case for which the spectral jumps in Doppler velocity are evident between 01:20 and 01:40 UT. There are also peaks in the SNR, coherence $|S_{12}|$ and the relative heights of the singular atmospheric scattering layers z_l and z_n which correspond to each other and thus, the "jumps" shown here have been interpreted by Chilson et al. (2000) as signatures of nonlinearly steepened gravity waves that move PMSE layers up and down. An explanation for the jumps has been proposed by Röttger et al. (1990d). They maintain that these discontinuities result when a thin scattering layer, that has been advected vertically by a steepened wave, is transported horizontally through the radar sampling volume. As atmospheric gravity waves propagate upwards, they experience an increase in amplitude. Once the amplitudes become large enough, they typically begin to break (Franke and Collins, 2003). However, the waves can become saturated, in which case they release just enough energy into turbulence to maintain a constant amplitude (Fritts et al., 1988). The waves can also exhibit a nonlinear transfer of energy from the fundamental wave frequency to higher frequency harmonics, in which case the wave amplitude continues to increase, but the structure of the wave becomes steepened or tilted (Chilson et al., 2000).

Another link between the PMSE and wave dynamics has been found when one considers 5-day planetary wave propagation in the summer mesosphere. Kirkwood et al. (2002) (Paper VI)

observed an amplification of the 5-day planetary wave in the summer high-latitude mesosphere, that has been previously predicted by the modelling work of Geisler and Dickinson (1976). It should be noted that, 5-day periodicities have been found earlier in noctilucent clouds (Sugiyama et al., 1996) and in PMSE (Kirkwood and Rechou, 1998). However, Kirkwood et al. (2002) (Paper VI) found a correlation of temperature variations with the 5-day wave and correspondence of these variations to PMSE occurrence. Particularly, a nearly linear relation between mean daily temperature and mean daily occurrence of PMSE has been established. The demonstrated sensitivity of PMSE to temperature fluctuations associated with 5-day waves suggested that 5-day planetary waves could modulate ice-aerosol formation at mesopause heights.

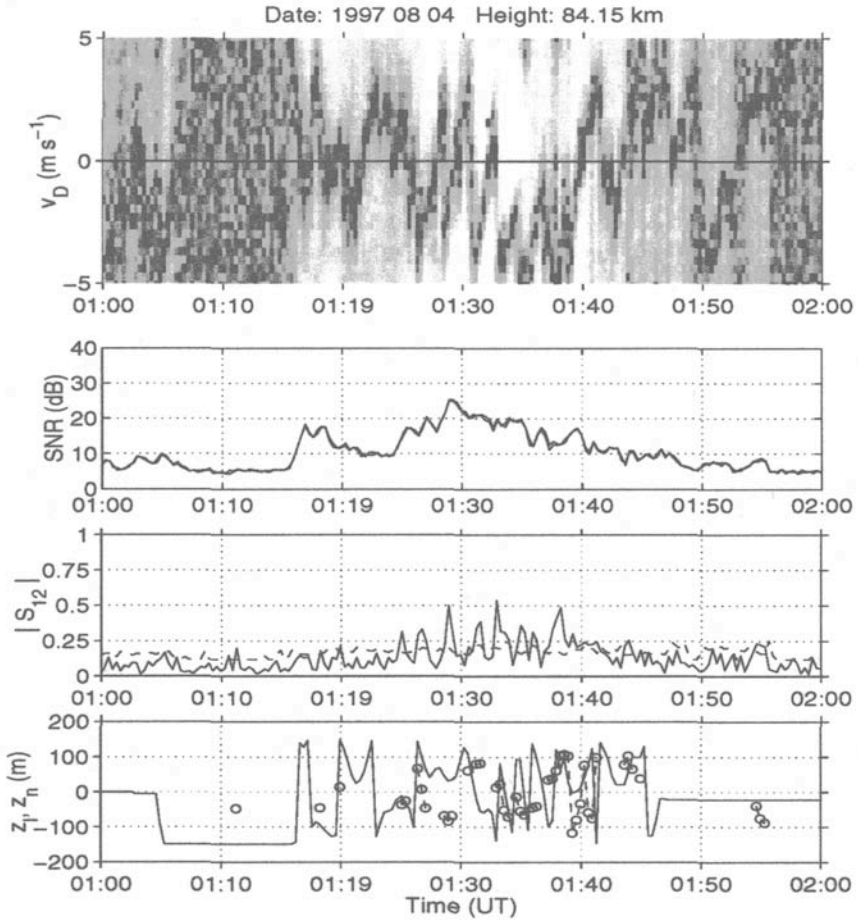

Figure 4.3. O*bservations of PMSE at height of 84.15 km, time period 01:00-02:00 UT on 4 August 1997. The upper panel shows the self-normalized spectrogram of Doppler velocities (v_D). The second panel shows traces of SNR for both frequencies plotted separately. The third panel shows traces of the FDI (frequency-domain interferometry) coherence (solid (line) and the 95% significance level (dashed line). The fourth panel shows the trace of z_l (circles) and z_n (solid line) (Chilson et al., 2000).*

4.3 Charged aerosols

PMSE might be divided into two categories: turbulent and non-turbulent (Cho and Kelley, 1993). The turbulent is related to neutral air turbulence and accounts for 10-30% of all observations (Lübken et al., 2002). But the majority of PMSE cases have been observed in the absence of

turbulence in the neutral air. Numerous investigations put forward different theories on non-turbulent PMSE type, namely: “dust hole scatter” (Havnes et al., 1992), “opalescence” (Trakhtengerts, 1994), “charged dust diffusive waves” (Hocking and Röttger, 1983), “vertical convergence” (Reid, 1997) and “plasma instabilities” (Blix, 1999). A detailed discussion of these theories would be beyond the scope of this thesis. However, the common feature of these theories is their need for the presence of charged aerosols to maintain significant fluctuations in the electron gas at scales around the Bragg scale (= radar half wavelength, 3 m for a 50 MHz radar) (Tatarskii, 1971).

The latest experimental results by Blix et al. (2003) confirm the main ideas of the mentioned above theories by demonstration a high degree of correlation between the PMSE echo power and the fluctuation intensity of electrons at scales comparable to half the radar wavelength. The PMSE in this study have been measured with the 224 MHz EISCAT VHF radar (69°N), 53.5 MHz ALOMAR-SOUSY VHF (69°N) and 53.5 MHz ALWIN VHF (69°N) radars. Recently, it has been generally accepted that such fluctuations are supported by the charged aerosols (Cho et al., 1992; Cho and Röttger, 1997; Rapp et al., 2002, 2003a, 2003b; Lie-Svedsen et al., 2003; Blix et al., 2003). Lie-Svedsen et al. (2003) define three main reasons why the aerosol particles can be essential for explanation of PMSE, namely: (1) low temperatures and water vapor availability in the polar summer mesopause allow the ice particles to grow, (2) charge aerosol number density is comparable to the local plasma density, and (3) aerosol’s low mobility “implies that small-scale structures in their distribution can persist for a long time without being smeared out by diffusion. Free electrons attach themselves easily to such particles, so that small-scale variations in particle density may be accompanied by similar small-scale variations of the free electron density, which in turn cause the PMSE”.

Studies of aerosol layers by sounding rockets experiments at summer mesopause indicate the presence of both positively and negatively charged aerosols associated with depletions in the electron number density profiles. The mean charge number density of such aerosols can be of order several 10^3 charges·cm^{-3} (Croskey et al., 2001; Havnes et al., 2001; Smiley et al., 2003). Lübken and Rapp (2001) and Rapp and Lübken (2001) developed a model that quantitatively determines the aerosol radii and number densities from the measurements of positive ion and electron number densities. They showed that nearly all combinations of electron and positive ion depletions and positive ion enhancements could exist depending on the properties of the aerosol particles and the background plasma conditions.

The aerosol radius might directly modify the strength of PMSE signal power. Rapp and Lübken (2003) modeled such conditions in the absence of the neutral air turbulence and showed that the decay time of electron perturbations is proportional to the square of the radius of the charged particles involved and the square of radar wavelength. Following this statement the radar signal decreases by 30 dB in 30 min. for aerosol radius of 10 nm, whereas for radius of 20 nm the same decrease takes 1.5-2 hours.

According to the experimental and model studies the optimal size of aerosols connected with PMSE varies from 10 nm (Havnes et al. 2001; Lie-Svedsen et al., 2003) to 30 nm (Lie-Svedsen et al., 2003). Particle with radii less than 10 nm might quickly diffuse and therefore remove the structure. For larger particles with radii 50-100 nm ion attachment instead of ambipolar diffusion become important, thus creating a correlation between electron and ion densities. This contradicts most *in situ* rocket measurements and, therefore, aerosols with large radii might be excluded from consideration (Lie-Svedsen et al., 2003).

The size of the aerosol particle determines the charge on its surface. The charge of an ice aerosol depends on the balance between the ion and electron content on its surface. Jensen and Thomas (1991) found a charge number of –1 for radii less than 10 nm, and a linearly increasing charge with the aerosol size, so that a particle with radius 0.1 μm would carry a charge of –4. If the ice is not pure but contaminated by metallic species, than the photoelectric component becomes important and the aerosol may become positively charged.

Cho et al. (1992) suggested that one of the most important effects of charged aerosols is the reduction of the electron diffusivity. If the electron diffusivity is considerably smaller than the kinematic viscosity of air, then fluctuations in the electron number density can extend to much smaller scales than the fluctuations of the turbulent velocity field and can, therefore, be erased mostly by the action of electron diffusion. Applying a multipolar diffusion theory of Hill (1978) to the diffusion system consisting of electrons, positive ions and charged aerosol particles, Cho et al. (1992) argued that PMSE can be created if more than 50% of all negative charge is bound on the aerosol particles, i.e. the ratio $\Box = Z_a N_a / N_e$ between the aerosol charge number density $Z_a N_a$ and the electron number density N_e is equal to 1.2 for negatively charge aerosols and 0.6 for positively charged aerosols. Under these circumstances the effective electron diffusion coefficient is close to the diffusion coefficient of aerosols. However, the values of $\Box$ contradict the experimental results by Blix et al. (2003), who showed that PMSE might also occur for rather small amounts of aerosols, with the number density of electrons exceeding the number of charged aerosols, i.e. $\Box$ is less 0.5. This fact has been also confirmed by Rapp and Lübken (2003), who found that, reduction of electron diffusivity almost independent of ratio between the aerosol charge number density and the electron number density. These authors suggested a "proxy " for the existence of PMSE observed by the VHF radar (Rapp et al., 2002). According to their model the radar reflectivity is proportional to the charge number density times the square of the aerosol radius. This proxy is valid in cases when there are enough free electrons left for the scattering of the VHF radar. However, in some cases when the electron number density is drastically diminished by the ice particles there might be an anticorrelation between the radar reflectivity and the charge number density (Blix et al., 2002). The difference to the conclusions of Cho et al. (1992) is most likely since only one type of positive ions and only a single size of aerosols instead of distribution were taken into account in the latter work.

Numerical simulations of aerosol particle perturbations in the mesopause region propose that, for aerosols structures on the order of a few meters, electron attachments and ambipolar diffusion might be the dominant processes, leading to small scale electron perturbations that can cause PMSE. The small-scale structures are able to persist as long as the aerosol layer persists. That process is likely to be limited by aerosol particle diffusion, which is on the order of hours (Lie-Svedsen et al., 2003).

So, as it is seen the topic is very complicated and the exact influence of aerosol on PMSE creation mechanism is still under discussion. Only direct measurements of aerosol population, size and charge distribution along with the neutral gas dynamics would clarify the questions on possible mechanisms behind the PMSE microphysics.

5. MST radar observation of the upper atmosphere

5.1 Scattering and reflection of MST radar signals in the upper atmosphere

MST (mesosphere-stratosphere-troposphere) radars are applied to study winds, waves, turbulence and instability in the atmosphere. They usually operate near 50 MHz and also called VHF radars (VHF-very high frequency band between 30 MHz and 300 MHz). The MST radars detect echoes from irregularities of the radio refractive index (Woodman and Guillen, 1974). The refractive index variations n, are directly related to variations of the atmospheric parameters: humidity, temperature, pressure and electron density, and can be expressed in the following equation:

$$n = 1 + \left[77.6 \cdot \frac{p}{T} + 3.75 \cdot 10^{5} \cdot \frac{e}{T^{2}} \right] 10^{-6} \quad 40.3 \cdot \frac{n_e}{f_o^{2}} ,$$

where e is the partial pressure of water vapor in mb, p is the atmospheric pressure in mb, T is the absolute temperature in K, n_e is the electron number density in m^{-3}, f_o is the radar operating frequency in Hz (Balsley and Gage, 1980)). At mesopause heights, i.e. at 80-90 km, the water vapor and pressure term are much smaller than the electron density term. So, the refractive index irregularities for MST radars are mostly determined by the electron density fluctuations, which have to exist at spatial scale of half the radar wavelength (3m for a 50 MHz radar). The electron density fluctuations in the mesosphere might be induced by perturbations in the ionization conditions, by neutral gas turbulence (Röttger, 1995) and by presence of highly hydrated ions (clusters) and aerosols (Cho and Kelley, 1993).

When atmospheric turbulence or small scale perturbations in the electron gas in the mesosphere mix the vertical profile of the refractive index and the associated gradients, fluctuations of n result, which in turn cause scattering and reflection of radar waves. The mean square fluctuations of the refractive index $<dn>^2$ is usually defined through the refractive index structure constant C_n^2 as:

$$C_n^2 = a \cdot \langle dn^2 \rangle \cdot L_o^{\frac{2}{3}},$$

where a is constant (| | 5) and L_o is the outer scale of turbulence in the inertial subrange. According to the classical theory of turbulence the inertial subrange is the cascade region where the kinematic energy spectrum depends only on the energy dissipation rate / , i.e. on dimensional grounds, the one-dimensional velocity fluctuation energy spectrum in the inertial subrange is proportional to $\varepsilon^{2/3} \cdot k^{-5/3}$, where k is the wavenumber. The three-dimensional spectrum, which corresponds to what the radar measures is proportional to $k^{-11/3}$. In the inertial subrange the large turbulence eddies decay into smaller eddies. A cutoff of the inertial subrange is determined by the inner scale l_o given as:

$$l_o = 9.9 \cdot \left(\frac{\nu^3}{\varepsilon} \right)^{\frac{1}{4}},$$

where $(\nu^3/\varepsilon)^{1/4}$ is the Kolmogorov microscale and ν is the kinematic viscosity. The outer scale L_o is proportional to the turbulence energy dissipation rate / and buoyancy or Brunt-Väisäillä frequency ω_B (Ottersten, 1969a):

$$L_o \mu \varepsilon^{\frac{1}{2}} \cdot \omega_B^{-\frac{3}{2}},$$

where square of the buoyancy frequency ω^2 is a measure of hydrostatic stability (Salby, 1996) and can be expressed in the form:

$$\omega^2 = g \cdot \frac{d \ln \theta}{dz},$$

where g is the gravitational acceleration, θ is the potential temperature, z is the altitude. The inner and outer scales of turbulence change as functions of altitude. Hocking (1985) has calculated the size of the inertial subrange of 10-100 m for the mesopause heights, i.e. between 80-90 km.

The radar reflectivity for scattering from a volume filled by isotropic turbulence in the inertial subrange according to Ottersten (1969b) is:

$$\eta = 0.38 \cdot C_n^2 \cdot \varepsilon^{\frac{1}{3}}$$

The received radar echo power P_s for isotropic volume scatter is given by the radar equation:

$$P_s = \frac{\lambda^2 A_E P_t \tau r}{8\pi r^2} \cdot \eta,$$

where P_t is the peak transmitter power, τ is the efficiency factor for the antenna transmission lines, A_E is the effective antenna area, r is the distance to the center of the scattering volume, Δr is the range gate width (Balsley and Gage, 1980).

If the radar receives echoes from steep vertical gradients of the refractive index, which might be observed by vertically beaming VHF radar, the power received by this partial reflection is:

$$P_r = \frac{\lambda^2 P_t A_E^2}{4\pi^2 r^2} \cdot \left| \eta^2 \right|,$$

where $|\eta^2|$ is the amplitude reflection coefficient (Gage et al., 1981).

Since it was not readily possible to discriminate between the different basic processes of scattering and partial reflection, detected by MST radar, it has become accustomed in the MST radar community to apply a nomenclature which is basing on the principal schematics of the different refractive index formations shown in Figure 5.1and summarized in Table 1 (Röttger, 1995).

Table 1. Model for scatter/reflection mechanisms of MST radar signals (Röttger, 1995).

Mechanism	Angular spectrum	Coherence time	Reflectivity structure
Bragg scatter (a) isotropic (b) anisotropic	 constant wide	 short short	random turbulence (a) isotropic (b) anisotropic
Fresnel scatter (a) stratified (b) spread	 narrow wide	 intermediate intermediate	multiple laminae (a) horizontally stratified (b) range, angle spread
Fresnel (partial) reflection (a) specular (b) diffuse	 narrow very narrow	 long very long	one dominating laminae in stable environment (a) very smooth (b) corrugated (rough)

The scattering mechanisms in MST radar applications are frequently called Bragg scatter, Fresnel scatter and Fresnel reflection. Bragg scatter is assumed to be the principal scattering mechanism for MST radar and is backscattering from spatial components at the Bragg wave number $k = 4\pi / \lambda$ of refractive index fluctuations in a turbulence layer, which is wider than the radar wavelength λ (Gossard and Strauch, 1983). The Bragg scatter can be isotropic, i.e. without causing a radar aspect sensitivity (radar echo power dependence on the zenith angle), if the turbulent irregularities of refractive index are homogeneously random and statistically similar in all directions. The anisotropic Bragg scatter causes an aspect sensitivity if the correlation distances between the irregularities are dependent on direction. Angular dependence for these two mechanisms is different, but the temporal variations are similar because of the randomly fluctuating irregularities.

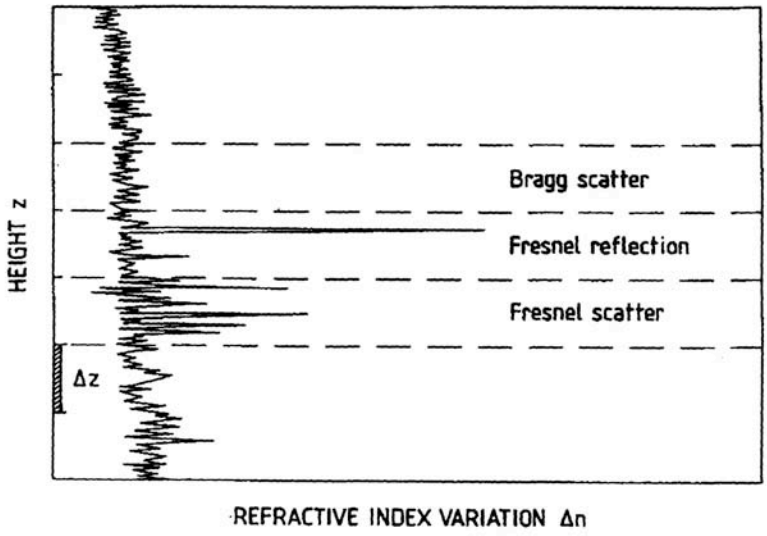

Figure 5.1. *Schematics of small-scale vertical variations of the refractive index showing the three main processes Bragg scatter, Fresnel scatter and Fresnel reflection. Δz is a typical range gate width (Röttger, 1995.)*

The terms Fresnel scatter and Fresnel reflection have been introduced to describe the condition that the horizontal correlation distance of the discontinuities is in the order of the Fresnel zone $(r \cdot \lambda)^{0.5}$, where r is the distance between the radar and the scatter/reflection volume, and λ is the radar wavelength. For correlation distances smaller than a fraction of the Fresnel zone Bragg scatter can dominate (Röttger, 1995). Fresnel scatter (Gage et al., 1981; Hocking and Röttger, 1983) occurs if, instead of random distributed irregularities, a few refractive index discontinuities in the vertical direction exist in the range gate. These discontinuities are randomly distributed in the vertical, but have a large extent in the horizontal direction. The radar echo characteristics resemble a distinct aspect sensitivity, but because the discontinuities are statistically independent, the temporal echo characteristics should be similar to those of Bragg scatter.

Fresnel reflection (Röttger and Larsen, 1990a) is observed if a single dominating discontinuity of the refractive index exists in the vertical direction, which has a large horizontal extent, similar to the case of Fresnel scatter. Aspect sensitivity expected to be observed. Vertical power profiles reveal large spikes, or thin and persistent structures, respectively. The temporal characteristics indicate long coherence time.

5.2 Esrange VHF MST Radar (ESRAD)

ESRAD (ESrange RADar) is a VHF MST radar located in northern Sweden (67°56'N, 21°04'E). It has been in near continuous operation since June 1996. The purpose of the radar is to provide information on the dynamic state of the atmosphere - winds, waves, turbulence and layering from the troposphere up to the lower thermosphere (ca. 1 km -110 km altitude). A summary of the radar's technical parameters is listed in Table 2.

ESRAD operates at a frequency of 52 MHz corresponding to a wavelength of 5.77 m. The transmitter consists of 72 1-kW solid-state modules that are grouped into 12 6-kW power blocks. The resulting peak power output power is 72 kW and the maximum duty cycle is 5%. Pulse repetition frequency rates from 100 Hz to 16 kHz are possible. Pulse lengths correspond to height resolutions between 150 m and 3 km. The radar is capable of pulse coding the transmitted signals using both Barker and complementary codes.

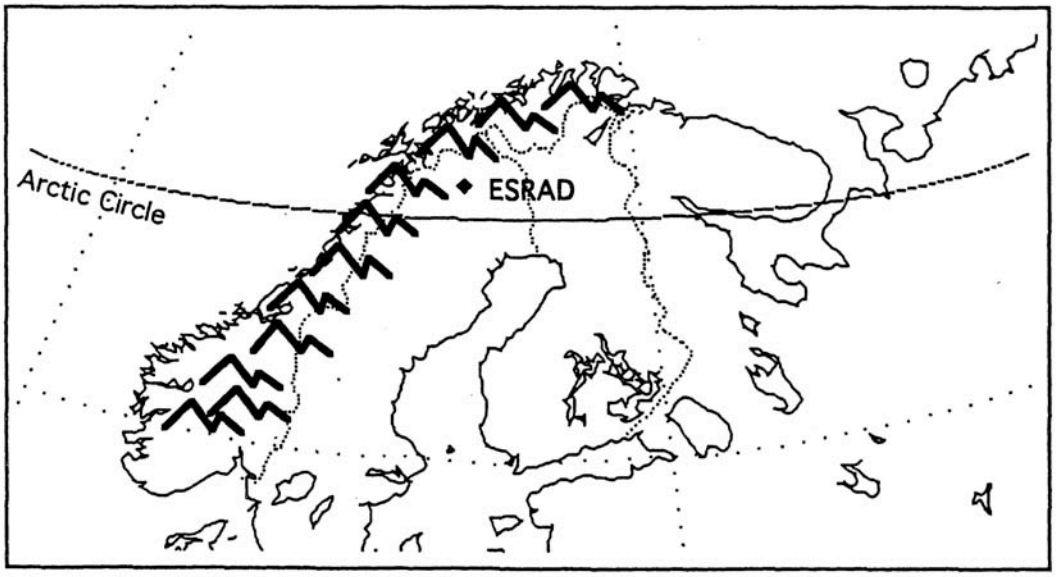

Figure 5.2. *Map showing the location of Esrange MST Radar (ESRAD) and the mountain chain in Northern Scandinavia (Kirkwood et al., 1997).*

The radar has 6 separate receivers for detection of backscattered signals from the atmosphere. The complex (in-phase and quadrature) data samples are recorded using a 12-channel data acquisition unit. The bandwidth of the separate receiving elements is 2 MHz. Using multiple receivers allows post-detection beam-steering and full spectral analysis of the returned signal. The digital processing system is able to process up to 256 heights per sample and integrates up to 4096 pulse repetitions per sample. The antenna consists of a 12 x 12 phased array of 5-element Yagis, each being approximately 6 m high. The Yagis are spaced about 4 m apart (corresponding to 0.7 times the radar wavelength). The 4 central positions in the array are not filled so as to allow for a small hut, containing the transmitters, receivers and control computer, to be located at the center of the array. Each group of 4 nearest neighbor Yagis is separately connected to the control house. This allows a large number of different antenna configurations using a patch board in the control house. It also gives the possibility for phase-steering of the beam to off zenith directions. The array is located so as to allow for possible future expansion in all directions.

The radar runs continuously, cycling between modes optimized for troposphere, stratosphere, or mesosphere. Special cycles, concentrating on one atmospheric region may be run from time to

time, for example, in support of rocket or balloon campaigns at Esrange. More detailed information can be found on the radar's homepage (http://www.irf.se/mst/EsrangeMST.html).

Table 2. Technical parameters of ESRAD MST radar (Chilson et al., 1999).

Transmitter	
Peak power	72 kW
Duty cycle	up to 5%
Frequency	52 MHz
Pulse repetition rate	100 Hz-16 kHz
Pulse length	1 μs – 50 μs
Coding	Complementary (2, 4, 8, 10, 16, 32, and 64 bits) and Barker (2, 3, 4, 5, 6, 7, 11, 13 bits)
Antenna	
Number of antennas	140
Antenna spacing	0.7λ
Antenna area	45 m x45 m
Beam swinging angles	7°, 14°, 20° in N, S, E, W directions
Power aperture product	$7 \cdot 10^6$ Wm^2
Receivers	
Configuration	6 separate receivers
Sampling interval	1 ms – 20 ms
Filters	250, 500, 1000, 2000 kHz
Digital Processing	
Number of height	1 - 256
Pre-integrations	1 – 4096 samples
Standard wind analysis	Spaced antenna and Doppler beam swinging

During the PMSE measurements ESRAD used a 16-bit complementary code having a baud length of 1 μS. This corresponds to height resolution of 150 m. The sampling frequency was set at 1450 Hz. The covered height range was 80-90 km. The presence of PMSE was determined on the basis of the radar SNR (signal-to-noise ratio). The echoes have been judged to be present if SNR exceeds –10 dB (Kirkwood et al., 1998 (Paper IV)) or –5 dB (Barabash et al., 1998 (Paper I)). The limit of –10 dB was found to represent the detection limit for the particular mode run, i.e. settings the limit 1 dB lower gave a large increase in false "signals", with uniform height distribution (Kirkwood et al., 1998 (Paper IV)). The limit of –5 dB was chosen such as to increase the confidence level for the data analysis. PMSE have been almost continuously observed with ESRAD during the summer period from late May until late August since 1997.

6. Summary of the included papers

Paper I. Barabash, V., Chilson, P., Kirkwood, S., Rechou, A., and Stebel, K., Investigations of the possible relationship between PMSE and tides using a VHF MST radar, Geophysical Research Letters, 25, 17, 3297-3300, 1998.

In Paper I the results obtained during the first complete season of PMSE observations using the Esrange MST radar are presented. The possible relationship between the PMSE, tidal winds and vertical wind shears is examined. Discrete time intervals have been chosen to investigate since there were considerable variations in the periodicities in the signal-to-noise ratio (SNR) of the PMSE and winds throughout the season. The seasonal variations of PMSE show a steep increase in occurrence at the end of May and fade-out in the middle of August. Horizontal wind measurements revealed terdiurnal, semidiurnal and diurnal tides. Very strong wind shears have been found. Nevertheless, since they did not show significant correlation with SNR, it was concluded that, the daily variation of the echoes is not determined by large scale wind shear producing turbulence, but rather by small scale dynamics and tidal effects on aerosols. Additionally, the wind shear seems not to be a necessary precondition for PMSE.

Paper II. Barabash, V., Kirkwood, S., and Chilson, P., Are variations in PMSE intensity affected by energetic particle precipitation? Annales Geophysicae, 20, 539-545, 2002.

Paper II addresses the question of the PMSE modification by extra ionization, added by precipitating energetic electrons from the magnetosphere or high energy particles from the Sun. Using the model of radar reflectivity and the absorption of the cosmic noise suggested by Klostermeyer (1999) the relation between the linear PMSE intensity and the square of absorption has been estimated by two different methods: by Pearson linear correlation and the Spearman rank correlation. The Pearson correlation coefficient reflects the strength of linear relationships, and the Spearman rank correlation reflects the strength of monotonic relationships. The obtained results demonstrate different levels of correlation when analyzing different data sets from the same time period, i.e. the mean diurnal variation and day-to day variations of PMSE. The mean diurnal variation of the square of absorption and the linear PMSE intensity are highly correlated. However, correlation between the linear signal-to-noise ratio and absorption on a day-to-day basis is rather weak and exceeds the confident levels only in the evening hours. This leads to the conclusion that, varying ionization cannot be considered as a primary source of varying PMSE. Nevertheless, since the height integrated radio wave absorption is not sufficient to describe the ionospheric conditions between 80-90 km, further investigations of the relationship between PMSE and energetic particles using direct measurements of electron/ ion number densities should be done.

Paper III. Barabash, V., Kirkwood, S., Feofilov, A., and Kutepov, A., Polar Mesosphere Summer Echoes during the July 2000 Solar Proton Event, Annales Geophysicae, (in press), 2003.

Paper III is concerned with solar proton events and PMSE. Because of the long duration of solar proton events it is possible to model the electron and ion number densities during day and night conditions using the observed proton fluxes and, thus, separate electron density dependence from solar illumination. The high level of electrons and ions maintained during the solar proton event allows us to test whether PMSE strength is related to the density of free electrons or to something else, such as the availability of the aerosols with different parameters. The observed PMSE revealed two distinguishing features: a substantial decrease in height for the PMSE lower limit in

the early morning hours, and decrease of the radar echoes above 86 km at the time of the greatest ionospheric disturbances. The results of numerical simulations demonstrated an increase of electrons and ions number densities throughout the event. The electric field calculated on the basis of magnetometer measurements and modelled conductivities gains its maximum of 91 mVm^{-1} during the most intensive period of geomagnetic disturbances. The electric field is expected to produce upward/downward transport of the ions, thus, possibly decreasing the amount of charged aerosols in the vicinity of PMSE. Since the calculated temperature increase was extremely small between 80-90 km altitude, it was concluded that, it is rather transport effects due to the intensified electric field at the most disturbed time which can be responsible for the reduction of PMSE above 86 km.

Paper IV. Kirkwood, S., Barabash, V., Chilson, P., Rechou, A., Stebel, K., Espy, P., Witt, G., and Stegman, J., The 1997 PMSE season - its relation to wind, temperature and water vapor, Geophysical Research Letters, 25, 11, 1867-1870, 1998.

Paper IV examines factors, which are considered to be the primary processes controlling the start and the end of PMSE season, namely mesospheric temperature, water vapor and stratospheric winds. The start of PMSE season is consistent with the water vapor increase at the end of May. Meanwhile the change of atmospheric circulation from eastward (winter) to westward (summer) as well as the temperature drop take place almost three weeks earlier. The end of PMSE season in August is characterized by simultaneous changes in all parameters. The possible explanations of this are that lower temperatures would be needed in early May to allow ice aerosols to form when less water vapor is available, or the aerosol might not have time to form before the temperature was forced above some threshold value. Other explanations are also possible. However, these lead to the suggestions that it is the aerosols, which are lacking at the beginning of the season and might determine the PMSE appearance. The increase of noctilucent clouds appearance in late July and August further supports this idea.

Paper V. Stebel, K., Barabash, V., Kirkwood, S., Siebert, J., and Fricke, K.H., Polar mesosphere summer echoes and noctilucent clouds: Simultaneous and common-volume observations by radar, lidar and CCD camera, Geophysical Research Letters, 27, 5, 661-664, 2000.

Paper V presents data from the first simultaneous and common-volume lidar, CCD camera and MST radar observations of PMSE and NLC during August 10/11 and 13/14 1997 in northern Sweden (68°N, 21°E). There was no direct temporal and spatial correlation of PMSE and NLC during the observations. However, similar wave like altitude variations seen in both phenomena at 10/11 August 1997 suggested a common dynamic regime between 82 and 89 km for this event. For the time interval 10/11 August the lidar and the CCD camera observed two NLC events with a different spatial orientation. The orientation of the NLC changed by about 90°, i. e. from southwest-northeast to southeast-northwest, which was also consistent with the wind direction derived from the MST radar observations. This fact gave evidence for advection of different air masses over the volume of measurements. Spatial parameters for NLC bands have been calculated as well.

Paper VI. Kirkwood, S., Barabash, V., Brändström, U., Moström, A., Stebel, K., Mitchell, N., and Hocking, W., Noctilucent clouds, PMSE and 5-day planetary waves: a case study, Geophysical Research Letters, 29, 10, 10.1029/2001GLO14022, 1-4, 2002.

The mesopause temperature at high latitudes depends not only on the general circulation but also on perturbations caused by waves including gravity waves, planetary waves and tides. 5–day periodicities have been reported in noctilucent clouds (Sugiyama et al., 1996) and PMSE (Sugiyama et al., 1996; Kirkwood and Rechou, 1998). In this paper the analysis of global meteorological assimilations between the middle of July and late August 2000 is presented. Observation of temperature, zonal winds and PMSE occurrence demonstrate the 5-day variability. The linear dependence of mean daily occurrence rate of PMSE on mean daily temperature indicates that the temperature is the primary factor controlling the PMSE occurrence. Since the PMSE have a strong daily variation, the observed 50 K span in mean daily temperatures between conditions giving 100% and 0% PMSE occurrence, respectively, might imply a similar temperature variability at PMSE heights over each day. The demonstrated sensitivity of PMSE to temperature fluctuations associated with 5-day waves supports the suggestion that 5-day planetary waves might significantly modulate ice-aerosol formation between 80-90 km height and thus, influence the PMSE appearance.

Bibliography

Akmaev, R., Simulation of large-scale dynamics in the mesosphere and lower thermosphere with the Doppler-spread parameterization of gravity waves, 2, Eddy mixing and the diurnal tide, J. Geophys. Res., 106, 1205-1213, 2001.

Andrews, D.G., Holton, J.R., and Leovy, C.B., Middle Atmospheric Dynamics, New York and London: Academic Press, 1987.

Balsley, B.B., and Gage, K.S., The MST radar technique: potential for middle atmospheric studies, J. Appl. Geophys., 118, 452-493, 1980.

Balsley, B.B., Ecklund, W.L., and Fritts, D.C., VHF echoes from the high-latitude mesosphere and lower thermosphere: Observations and interpretations, J. Atmos. Sci., 40, 2451-2466, 1983.

Balsley, B.B., Woodman, R.F., Sarango, m., Rodriguez, R., Urbina, J., Ragaini, E., Carey, J., Huaman, M., and Giraldez, A., On the lack of southern hemisphere polar mesosphere summer echoes, J. Geophys. Res., 100, 11685-11693, 1995.

Barabash, V., Chilson, P., Kirkwood, S., Rechou, A., and Stebel, K., Investigations of the possible relationship between PMSE and tides using a VHF MST radar, Geophys. Res. Lett., 25, 17, 3297-3300, 1998.

Barabash, V., Kirkwood, S., and Chilson, P., Are variations in PMSE intensity affected by energetic particle precipitation?, Ann. Geophys., 20, 539-545, 2002

Barabash, V., Kirkwood, S., Feofilov, A., and Kutepov, A., Polar Mesosphere Summer Echoes during the July 2000 Solar Proton Event, Ann. Geophys. (in press), 2003.

Berger, U., and Von Zahn, U., The two-level structure of the mesopause: A model study, J. Geophys. Res., 104, 22083-22093, 1999.

Blix, T.A., Is there a connection between polar mesosphere summer echoes and the existence of plasma instabilities in the E-layer, in Proceedings of the 14th ESA Symposium on European Rocket and Balloon Programmes and Related Research, Potsdam, Germany (ESA SP-437), Neuilly, France, 1999.

Blix, T.A., Rapp, M., and Lübken, F.J., Relations between small scale electron number density fluctuations, radar backscatter and charged aerosol particles, J. Geophys. Res., 2002.

Blix, T.A., Rapp, M., and Lübken, F.J., Relations between small scale electron number density fluctuations, radar backscatter and charged aerosol particles, J. Geophys. Res., 2003.

Brasseur, G., and Solomon, S., Aeronomy of the Middle Atmosphere, D. Reidel Publishing Company, Dordrecht, Holland, 1986.

Bremer, J., Hoffmann, P., and Hansen, T.L., Geomagnetic control of polar mesosphere summer echoes, Ann. Geophys., 18, 202-208, 2000.

Carter, D.A., and Balsley, B.B., The summer wind field between 80 and 93 km observed by the MSt radar at Poker Flat, Alaska (65°N), J. Atmos. Sci., 39, 2905-2915, 1982.

Chilson, P.B., Czechowsky, P., Klostermeyer, J., Rüster, R., and Schmidt, G., An investigations of measured temperature profiles and VHF mesosphere summer echoes at mid-latitudes, J. Geophys. Res., 102, 23819-23828, 1997.

Chilson, P., Kirkwood, S., and Nilsson, A., The Esrange MST radar: a brief introduction and procedure for range validation using balloons, Radio Sci., 34, 2, 427-436, 1999.

Chilson, P., Kirkwood, S., and Häggström, I., Frequency-domain interferometry mode observations of PMSE using the EISCAT VHF radar, Ann., Geophys., 2000.

Cho, J.Y.N., Hall, T.M., and Kelley, M.C., On the role of charged aerosols in polar mesosphere summer echoes, J. Geophys. Res., 97, 875-886, 1992.

Cho, J.Y.N., and Kelley, M.C., Polar mesosphere summer echoes: Observations and current theories, Rev., Geophys., 31, 243-265, 1993.

Cho, J.Y.N., and Morley, R.L., PMSE dependence on long-period vertical motions, Geophys. Res. Lett., 22, 1197-1200, 1995.

Cho, J.Y.N., and Röttger, J., An updated review of polar mesosphere summer echoes: Observation, theory, and their relation to noctilucent clouds and sub-visible aerosols, J. Geophys., Res., 102, 2001-2020, 1997.

Croskey, C.L., Mitchell, J.D., Friedrich, M., Torkar, K.M., Hopper, U.-P., and Goldberg, R.A., Electrical structure of PMSE and NLC regions during the DROPPS program, Geophys. Res. Lett., 28, 1427-1430, 2001.

Czechowsky, P., Rüster, R., and Schmidt, G., Variations of mesospheric structures in different seasons, Geophys. Res. Lett., 6, 459-462, 1979.

Czechowsky, P., Reid, I.M., Rüster, R., and Schmidt, G., VHF radar echoes observed in the summer and winter polar mesosphere over Andoya, Norway, J. Geophys. Res., 94, 6199-5217, 1989.

Ecklund, W.L., and Balsley, B.B., Long-term observations of the arctic mesopause with the radar at Poker Flat, Alaska, J. Geophys. Res., 86, 7775-7780, 1981.

Fiedler, J., Baumgarten, G., and von Cossart, G., Noctilucent clouds above the ALOMAR between 1997 and 2001: occurrence and properties, J. Geophys. Res., 2002.

Franke, S.J., Röttger, J., LaHoz, C., and Liu, C.H., Frequency domain interferometry of polar mesosphere summer echoes with the EISCAT VHF radar: a case study, Radio Sci., 27, 417-428, 1992.

Franke, P.M., and Collins, R.L., Evidence of gravity wave breaking in lidar data from the mesopause region, Geophys. Res. Lett., 30, 4, 1155, doi:10.1029/2001GL014477, 2003

Fritts, D.C., Smith, S.A., Balsley, B.B., and Philbrick, C.R., Evidence of gravity wave saturations and local turbulence production in the summer mesosphere and lower thermosphere during the STATE experiment, J. Geophys. Res., 93, 7015-7025, 1988.

Gadsden, M. and Schröder, G., Noctilucent Clouds, Springer Verlag, Berlin Heidelberg, 1989.

Gage, K.S., Balsley, B.B., and Green, J.L., Fresnel scattering model for the specular echoes observed by VHF radar, Radio Sci., 16, 1447-1453, 1981.

Garcia, R.R., and Solomon, S., The effects of breaking gravity waves on the dynamics and chemical composition of the mesosphere and lower thermosphere, J. Geophys. Res., 90, 3850-3868, 1985.

Geisler, J.E., and Dickinson, R.E., The five-day wave in a sphere with realistic zonal winds, J. aymos. Sci., 33, 632-641, 1976.

Gossard, E.E and Strauch, R.G., Radar observations of clear air and clouds, Elsevir Publ. Comp, 1983.

Havnes, O., Melandsö, F., Hoz, C.L., Aslaksen, T.K., and Hartquist, T., Charged dust in the Earth's mesopause: effects on radar backscatter, Phys. Sci., 45, 535-544, 1992.

Havnes, O., Brattli, A., Aslaksen, T., Singer, W., Latteck, R., Blix, T., Thrane, E., and Tröim, J., First common-volume observations of layered plasma structures and polar mesosphere summer echoes by rocket and radar, Geophys. Res. Lett., 28, 1419-1422, 2001.

Hill, R.J., Nonneutral and quasi-neutral diffusion of weakly ionized multiconstituent plasma, J. Geophys. Res., 83, 989-998, 1978.

Hocking, W.K., and Röttger, J., Pulse length dependence of radar signal strengths for Fresnel backscatter, Radio Sci, 18, 1312-1324, 1983.

Hocking, W.K, Measurements of turbulent energy dissipation rates in the middle atmosphere by radar techniques: A review, Radio Sci., 20, 1403-1422, 1985.

Hocking, W.K., Middle atmosphere dynamical studies T Resolute Bay over a full year: Mean winds, tides and special oscillations, J. Atmos. Sol. Terr. Phys., 2002.

Hoffmann, P., Singer, W., and Bremer, J., Mean seasonal and diurnal variations of PMSE and winds from 4 years of radar observations at ALOMAR, Geophys. Res. Lett., 26, 11, 1525-1528, 1999.

Hoppe, U.-P., Hall, C., and Röttger, J., First observations of summer polar mesospheric backscatter with a 224 MHz radar, Geophys. Res. Lett., 15, 28-31, 1988.

Huaman, M., and Balsley, B.B., Differences in near-mesopause summer winds, temperatures, and water vapor at northern and southern latitudes as possible causal factors for inter-hemispheric PMSE differences, Geophys. Res. Lett., 26, 11,1529-1532, 1999.

Jacobi, Ch., Schminder, R., and Kürschner, D., Planetary wave activity obtained from long-period (2-18 days) variations of mesopause region winds over central Europe (52°N, 15°E), J. Atmos. Sol.Terr. Phys., 60, 1, 81-93, 1998.

Jensen, E., and Thomas, G.E., Charging of mesospheric particles: implication of electron density and particle coagulation, J. Geophys. Res., 96 (18), 603-618, 1991.

Jiyao Xu, Smith, A.K., and Ruiping Ma, A numerical study of the effect of gravity-wave propagation on minor species distributions in the mesopause region, J. Geophys. Res., 108-D3, 4119, 10.1029/2001JD001570, 2003.

Karashtin, A.N., Shlyugaev, Y.V., Abramov, V.I., Belov, I.I., Berezin, I.V., Bychkov, V.V., Eryshev, E.B., and Komrakov, G.P., First HF radar measurements of the summer mesopause echoes at SURA, Ann. Geophys., 1996.

Kelley, M.C., Farley, D.T., and Röttger, J., The effects of cluster ions on anomalous VHF backscatter from the summer polar mesosphere, Geophys. Res. Lett., 14, 1031-1034, 1987.

Klostermeyer, J., On the diurnal variation of polar mesosphere summer echoes, Geophys. Res. Lett., 26 (21), 3301-3304, 1999.

Kirkwood, S., Rechou, A., Stebel, K., Barabash, V., Chilson, P., Marcus L., and Olsen, P.E., Wind profiling with ESRAD, the Esrange MST radar, Proceedings fo COSt-76 Profiler workshop 1997, Engelberg, Switzerland, May 1997.

Kirkwood, S., Barabash, V., Chilson, P., Rechou, A., Stebel, K, Espy, P., Witt, G., and Stegman, J., The 1997 PMSE season - its relation to wind, temperature and water vapor, Geophys. Res. Lett., 25, 1867-1870, 1998.

Kirkwood, S., and Rechou, A., Planetary wave modulation of PMSE, Geophys. Res. Let., 25, 4509-4512, 1998.

Kirkwood, S., Barabash, V., Brändström, U., Moström, A., Stebel, K., Mitchell, N., and Hocking, W., Noctilucent clouds, PMSE and 5-day planetary waves: a case study, Geophys. Res. Lett., 1-4, 2002.

Kirkwood, S., and Stebel, K., Influence of planetary waves on noctilucent cloud occurrence over NW Europe, J. Geophys. Res., 208, D8, 10.1029/2002JD002356, 2003.

Körner, U., and Sonnemann, G.R., Global 3D-modelling of the water vapor concentration of the mesosphere/mesopause region and implications with respect to the NLC region, J. Geophys. Res., 106, 9639-9651, 2001.

Latteck, R., Singer, W., and Höffner J., Mesosphere summer echoes as observed by VHF radar at Kühlungsborn, (54°N), Geophys. Res. Lett., 26, 11, 1533-1536, 1999.

Lie-Svedsen, O., Blix,, T.A., Hopper, U.-P., and Thrane, E.-V., Modelling the plasma response to small-scale aerosol particle perturbations in the mesopause region, J. Geophys. Res., 108, D8, 8442, doi:10.1029/2002JD002753, 2003.

Luo, Y., Manson, A.H., Meek, C.E., Meyer, C.K., and Forbes, J.M, The quasi 16-day oscillations in the mesosphere and lower thermosphere at Saskatoon (52°N, 107°W), 1980-1996, J. Geophys. Res., 105, 2125-2138, 2000.

Luo, Y., Manson, A.H., Meek, C.E.,Meyer, C.K., Burrage, M.D., Fritts, D.C., Hall, C.M., Hocking, W.K., MacDougall, J., Riggin, D.M., and Vincent, R.A., The 16-day planetary waves: multi-Mf radar observations from the arctic to equator and comparisons with the HRDO measurements and the GSWM modeling results, Ann. Geophys., 20, 691-709, 2002.

Lübken, F.J., Fricke, K.-H. and Langer, M., Noctilucent clouds and the thermal structure near the arctic mesopause, J. Geophys. Res., 101, 9489-9508, 1996.

Lübken, F.J., Seasonal variation of turbulent energy dissipation rates at high latitudes as determined by *in situ* measurements of neutral density fluctuations, J. Geophys. Res., 102, 13441-13456, 1997.

Lübken, F.J., and von Zahn, U., Thermal structure of the mesosphere region at polar latitudes, J. Geophys. Res, 96, D11, 20841-20857, 1991

Lübken, F.J., Thermal structure of the Arctic summer mesosphere, J. Geophys. Res.,104, D8, 9135-9149, 1999.

Lübken, F.J., and Rapp, M., Modeling of particle charging in the polar summer mesosphere: Part 2-Application to measurements, J. Atmos. Solar. Terr. Phys., 63, 771-780, 2001.

Lübken, F.J.,, Rapp, M., and Hoffmann, P., Neutral air turbulence and temperatures in the vicinity of polar mesosphere summer echoes, J. Geophys. Res., 2002.

Lübken, F.J., and Müllemann, A., First *in situ* temperature measurements in the summer mesopause at very high latitudes, J. Geophys. Res., 108, D8, 8448, 1029/2002JD002414, 2003.

Manson, A.H., and Meek, C.E., Climatologies of mean winds and tides observed by medium frequency radars at Tromsö (70°N) and Saskatoon (52°N) during 1987-1989, Ca, J. Phys., 69, 966-975, 1991.

Manson, A.H. et al., Seasonal variations of the semidiurnal and diurnal tides in the MLT: Multi-year Mf radar observations from 2 to 70°N and the GSWM tidal model, J. Atmos. Sol. Terr. Phys., 61, 809-828, 1999.

Manson, A.H., Meek, C.E., Hall, C.M., Nozawa, S., Mitchell, N.J., Pancheva, D., Singer, W., and Hoffman, P., Mesopause dynamics from the Scandinavian triangle of radars within the PSMOS-DATAR project, Ann. Geophys., 2003.

Marti, J., and Mauersberger, K., A survey and new measurements of ice vapor pressure at temperatures between 170 and 250 K, Geopys. Res. Lett., 20, 363-366, 1993.

Medvedev, A.S., and Klaassen, G.P., Thermal effects of saturation gravity waves in the atmosphere, J. Geophys. Res., 108, D2, 4040, 10.10292002JD002504, 2003.

Mitchell, N.J., Pancheva, D., Middleton, H.R., and Hagan, M.E., Mean winds and tides in the Arctic mesosphere and lower thermosphere, J. Geophys. Res., 107, A1, 10.1029/2001JA900127, 2002.

Nussbaumer, V., Fricke, K.H., Langer, M., Singer, W., and von Zahn, U., First simultaneous and common volume observations of noctilucent clouds and polar mesosphere summer echoes by lidar and radar, J. Geophys. Res., 101, D14, 19,161-19,167, 1996.

Ottersten, H., Atmospheric structure and radar backscattering in clear air, Radio Sci., 4, 1179-1193, 1969a.

Ottersten, H., Radar backscattering from the turbulent clear atmosphere, Radio Sci., 4, 1251-1255, 1969b.

Pan, C.J., and Röttger, J., Structures of polar mesosphere summer echoes observed with the EISCAT VHF radar in the interferometer mode, in Solar-Terrestrial Enrgy Program: Proceedings of the Seventh Workshop on Technical and Scientific Aspects of MST radar, 252-255, SCOSTEP Secretariat. Boulder Colo., 1996.

Portnyagin, Y.I., Forbes, J.M., Fraser, G.J., Vincent, R:A., Avery, S.K., Lysenko, I.A., and Makarov, N.A., Dynamics of the Antarctic and Arctic mesosphere and lower thermosphere regions, I, The prevailing wind, J. Atmos., Terr. Phys., 55, 827-841, 1993a.

Portnyagin, Y.I., Forbes, J.M., Fraser, G.J., Vincent, R.A., Avery, S.K., Lysenko, I.A., and Makarov, N.A., Dynamics of the Antarctic and Arctic mesosphere and lower thermosphere regions, I, The semidiurnal tide, J. Atmos., Terr. Phys., 55, 843-855, 1993b.

Portnyagin, Y.I., and Solovjova, T.V., Global empirical wind model for the upper mesosphere/ lower thermosphere, I, Prevailing wind, Ann. Geophys., 18, 300-315, 2000.

Rapp, M., and Lübken, F.J., Modelling of particle charging in the polar summer mesosphere: Part 1-General results, J. Atmos. Solar. Terr. Phys., 63, 759-770, 2001.

Rapp, M., Gumbel, J., Lübken, F.J., and Latteck, R., D-region electron number density limits for the existence of polar mesosphere summer echoes, J. Geophys. Res., 2002.

Rapp, M., Lübken, F.J., Müllemann, A., Thomas, G.E., and Jensen, E.J., Small scale temperature variations in the vicinity of NLC: experimental and model results, J. Geophys. Res., 2003a.

Rapp, M., Lübken, F.J., and Blix, T., The role of charge ice particles for the creation of PMSE: a review of recent developments, Adv. Space res., 2003b.

Rapp, M., and Lübken, F.J., On the nature of PMSE: electron diffusion in the vicinity of charged particles revisited, J. Geophys. Res., 108, D8, 8437, 10.1029/2002JD002857, 2003.

Reid, G.C., Vertical wind convergence and the formation of aerosol layers in the upper mesosphere, Geophys. Res. Lett., 24, 1997.

Reid, I M., Rüster, R., Czechowsky, P., and Schmidt, G., VHF radar measurements of momentum flux in the summer polar mesosphere over Andenes (69°N, 16°E), Norway, Geophys. Res. Lett., 15, 1263-1266, 1988.

Reid, I M., Czechowsky, P., Rüster, R., and Schmidt, G., First VHF radar measurements of mesopause summer echoes at mid-latitudes, Geophys. Res. Lett., 16, 135-138, 1989.

Richmond, A.D., Ionosphere-thermosphere interactions at high latitudes, , In Incoherent scatter: theory, practice and science, collections of lectures given in Cargesica, Technical report 97/53, EISCAT Sci. Ass., 1995.

Röttger, J., La Hoz, C., Kelley, M.C., Hoppe, U.-P., and Hall, C.: The structure and dynamics of polar mesospheric summer echoes observed with the EISCAT 224 MHz radar, Geophys. Res. Lett., 15, 1353-1356, 1988.

Röttger, J. and Larsen, M.F., UHF/ VHF radar techniques for atmospheric research and wind profiler applications, in Radar on Meteorology, American Met, Soc., 235-281. 1990a.

Röttger, J. and La Hoz, C., Characteristics of polar mesosphere summer echoes (PMSE) observed with the EISCAT 224 MHz radar and possible explanation of their origin, J. Atmos. Terr. Phys., 52, 893-906, 1990b.

Röttger, J., Rietveld, M.T., La Hoz, C., Hall, C., Kelley, M.C., and Swartz, W., Polar mesosphere echoes observed with the EISCAT 933 MHz radar and the CUPRI 46.9 MHz radar, their similarity to 224 MHz radar echoes and their relation to turbulence and electron density profiles, Radio Sci., 25, 671-687, 1990c.

Röttger, J., La Hoz, C., Franke,, S.J., and Liu, C.H., Steepening of reflectivity structures detected in high-resolution Doppler spectra of polar mesosphere summer echoes (PMSEI observed with the EISCAT 224 MHz radar, J. Atmos. Terr. Phys., 52, 939-954, 1990d.

Röttger, J., Radar observations of the middle and lower atmosphere, In Incoherent scatter: theory, practice and science, collections of lectures given in Cargesica, Technical report 97/53, EISCAT Sci. Ass., 1995.

Rüster, R., VHF radar observations of non-linear interactions in the summer polar mesosphere, J. Atmos. Terrr. Phys., 56, 1289-1299, 1994.

Rüster, R., Velocity and associated echo power variations in the summer polar mesosphere, Geophys. Res. Lett., 22, 65.67, 1995.

Salby, M.L., Fundamentals of Atmospheric Physics, Academic Press Inc., 1996.

Smiley, B., Robertson, S., Horanyi, M., Blix, T., Rapp, M., Latteck, R., and Gumbel, J., Measurements of positively and negatively charged particles inside PMSE during MIDA SOLSTICE 2001, J. Geophys. Res., 108, 0, doi:10.1029/2002JD002425, 2003.

Smith, W.S., Theon, J.S., Swartz, P.C., Katchen, L.B., and Horvath, J.J., Temperature, pressure, density and wind measurements in the stratosphere and mesosphere, 1966, NASA TRR-288, 1968.

Smith, W.S., Theon, J.S., Swartz, P.C., Casey, J.F., and Horvath, J.J., Temperature, pressure, density and wind measurements in the stratosphere and mesosphere, 1967, NASA TRR-316, 1969.

Stebel, K., Barabash, V., Kirkwood, S., Siebert, J., and Fricke, K.H., Polar mesosphere summer echoes and noctilucent clouds: Simultaneous and common-volume observations by radar, lidar and CCD camera, Geophys. Res. Letts, 27, 5, 661-664, 2000.

Sugiyama, T., Murako, Y., Sogawa, H., and Fukao, S., Oscillation in polar mesosphere summer echoesand bifurcation of noctilucent cloud formation, Geophys. Res. Let., 23, 63-656, 1996.

Swinbank, R., and O'Neil, A., A stratosphere-troposphere data assimilation system, Monthly Weather Review, 122, 686-702, 1994.

Tatarskii, V.I., The effect of the turbulent atmosphere on wave propagation, Isr. Program for Sci Transl., Jerusalem, 1971.

Thomas, L., Astin, I., and Prichard, T., The characteristics of VHF echoes from the summer mesopause region at mid-latitudes, J. Atmos. Terr. Phys., 54, 969-977, 1992.

Thomas, L., and Astin, I., The form of metre-scale turbulence at mesopause heights in summer, J. Atmos. Terr. Phys., 56, 467-478, 1994.

Thomas, G.E., Climatology of polar mesospheric clouds: Interannual variability and implications for long-term trends, in the upper mesosphere and lower thermosphere: A review of experiment and theory, Geophys. Monagr. Ser., 87, ed. by R.M. Johnson and T.L.Killeen, 185-200, AGU, Washington D.C., 1995.

Trakhtengerts, V.Y., Generation mechanisms of polar mesosphere summer echoes, J. Geophys. Res., 99, 21083- 21088, 1994.

Vincent, R.A., Gravity wave motions in the mesosphere and lower thermosphere observed at Mawson, Antarctica, J. Atmos. Terr. Phys., 56, 593-602, 1994.

Virdi, T.S., and Williams, P.J.S., Altitude variations in the amplitude and phase of tidal oscillations at high latitudes, J. Atmos. Terr. Phys., 55, 697-717, 1993.

Von Zahn, U., Achievements of ALOMAR, ESA-SP 397, 141-162, 1997.

Von Zahn, U., and Bremer, J., Simultaneous and common-volume observations of noctilucent clouds and polar mesosphere summer echoes, Geophys. Res. Lett., 26, 11, 1521-1524, 1999.

Witt, G., Height, structure and displacements of noctilucent clouds, Tellus 14, 1-18, 1962.

Williams, C.R., and Avery, S.K., Analysis of long-period waves using the mesosphere-stratosphere-troposphere radar at Poker Flat, Alaska, J. Geophys. Res., 97, 855-861, 1992.

Williams, P.J.S., Jones, G.O.L., Palmer, J.R., and Risbeth, H., The association of polar mesosphere summer echo layers with tidal modes, Ann. Geophys., 13, 454-457, 1995.

Woodman, R.F, and Guillen, A, Radar observations of winds and turbulence in the stratosphere and mesosphere, J. Atmos. Sci., 31, 493-505, 1974.

Woodman, R.F, Balsley, B.B., Aquino, F.A., Flores, L., Vazquez, E., Arango, M., Huaman, M., and Soldi, H., First observations of PMSE in Antarctica, J. Geophys. Res., 1999.

Zhu, X., Yee, J.H., and Talaat, E.R., Diagnos and dynamics and energy balance in the mesosphere and lower thermosphere, J. Atmos. Sci., 58, 2441-2454, 2001.

Acknowledgements

First of all I would like to thank the Swedish Institute of Space Physics, IRF for offering me the opportunity to take my PhD in Kiruna. The studies have been financed by the EU project Space and Environment Institute (MRI), Atmospheric Physics Program, Swedish Science Research Council (NFR/VR) and the Swedish Institute of Space Physics.

I am greatly indebted to my supervisor Prof. Sheila Kirkwood for her support during my studies. Special thanks to Dr. Phillip Chilson from the National Oceanic and Atmospheric Administration, USA for being my assistant supervisor and for many valuable discussions.

I am very grateful to all my colleagues at IRF in Kiruna for providing an excellent working environment. Many thanks to Arne Moström, Stefan Vanhaniemi and Dr. Hans Nilsson for their help in solving the computer problems. Special thanks to Birgitta Määttä, and Torbjörn Lövgren for all help in preparation of this thesis.

I would like to thank the personnel of Esrange, Swedish Space Corporation and particularly the Science coordinator Ola Widell for Esrange VHF MST radar (ESRAD) operation.

I finally want to express my appreciation to my family for continuously encouraging me to get this thesis finished.

Acronyms

ACE	Advanced Composition Explore satellite, Office of Space Science Mission and Payload Development Division of the National Aeronautics and Space Administration
ALOMAR	Artic Lidar Observatory for Middle Atmospheric Research
CCD	Charge-Coupled Device
CIRA	COSPAR International Reference Atmosphere model
COSPAR	Committee on Space Programs and Research
CRISTA1, 2	Cryogenic Infrared Spectrometers and Telescopes for the Atmosphere
EISCAT	European Incoherent Scatter Scientific Association
ESRAD	ESrange RADar
Esrange	European Space Launching Range (European Space Agency)
FDI	Frequency-domain interferometry
GOES-10	Geostationary Satellite, National Oceanic and Atmospheric Administration, US Department of Commerce
HALOE	HALogen Occultation Experiment, Upper Atmosphere Research Satellite spacecraft
MSISE-90	Mass-Spectrometer-Incoherent-Scatter empirical model
MST	Mesosphere-Stratosphere-Troposphere
NLC	Noctilucent Clouds
NOAA	National Oceanic and Atmospheric Administration
PMSE	Polar Mesosphere Summer Echoes
ppmv	Parts per million by volume
SKiYMET	All-Sky Interferometric Meteor Radar
SNR	Signal-to-Noise Ratio
SOUSY	SOUnding SYstem
UARS	Upper Atmosphere Research Satellite, Office of Space Science Mission and Payload Development Division of the National Aeronautics and Space Administration
VHF	Very High Frequency band between 30 MHz and 300 MHz
UHF	Ultra High Frequency band between 300 MHz and 3000 MHz
UKMO	UK Meteorological Office
UT	Universal Time